Available online at www.sciencedirect.com
ScienceDirect
Geomorphology 82 (2006) 58–83
GEOMORPHOLOGY
www.elsevier.com/locate/geomorph

The role of sediment in controlling steady-state bedrock channel slope: Implications of the saltation–abrasion incision model

Leonard S. Sklar [a,*], William E. Dietrich [b]

[a] Department of Geosciences, San Francisco State University, 1600 Holloway Avenue, San Francisco, CA 94132, USA
[b] Department of Earth and Planetary Science, University of California, Berkeley, CA 94720, USA

Received 4 April 2004; received in revised form 30 August 2005; accepted 30 August 2005
Available online 13 July 2006

Abstract

The saltation–abrasion model is a mechanistic model for river incision into bedrock by saltating bedload, which we have previously derived and used experimental data to constrain all parameter values. Here we develop a method for applying the saltation–abrasion model at a landscape scale, and use the model as a reference for evaluating the behavior of a wide range of alternative incision models, in order to consider the implications of the saltation–abrasion model, as well as other models, for predicting topographic steady-state channel slope. To determine the single-valued discharge that best represents the effects of the full discharge distribution in transporting sediment and wearing bedrock, we assume all runoff can be partitioned between a low-flow and a high-flow discharge, in which all bedload sediment transport occurs during high flow. We then use the gauged discharge record and measurements of channel characteristics at a reference field site and find that the optimum discharge has a moderate magnitude and frequency, due to the constraints of the threshold of grain motion and bed alluviation by high relative sediment supply. Incision models can be classified according to which of the effects of sediment on bedrock incision are accounted for. Using the predictions of the saltation–abrasion model as a reference, we find that the threshold of motion is the most important effect that should be represented explicitly, followed in order of decreasing importance by the cover effect, the tools effect and the threshold of suspension effect. Models that lack the threshold of motion over-predict incision rate for low shear stresses and under-predict the steady-state channel slope for low to moderate rock uplift rates and rock strengths. Models that lack the cover effect over-predict incision rate for high sediment supply rates, and fail to represent the degree of freedom in slope adjustment provided by partial bed coverage. Models that lack the tools effect over-predict incision rate for low sediment supply rates, and do not allow for the possibility that incision rate can decline for increases in shear stress above a peak value. Overall, the saltation–abrasion model predicts that steady-state channel slope is most sensitive to changes in grain size, such that the effect of variations in rock uplift rate and rock strength may affect slope indirectly through their possible, but as yet poorly understood, influence on the size distribution of sediments delivered to channel networks by hillslopes.

Keywords: Rivers; Erosion; Sediment supply; Grain size; Magnitude–frequency; Landscape evolution

1. Introduction

1.1. Motivation

One of the central problems in understanding the relief structure and topographic texture of tectonically

* Corresponding author. Tel.: +1 415 338 1204; fax: +1 415 338 7705.
E-mail address: leonard@sfsu.edu (L.S. Sklar).

0169-555X/$ - see front matter © 2006 Elsevier B.V. All rights reserved.
doi:10.1016/j.geomorph.2005.08.019

active landscapes is the question of what controls the slope of an actively incising bedrock channel. Previous work over several decades has led to an understanding of the dynamics of slope adjustment in alluvial channels (e.g. Mackin, 1948; Schumm, 1973; Bull, 1979; Snow and Slingerland, 1987), in which slope is controlled by the long-term balance between sediment supply and sediment transport capacity. Howard (1980) identified two distinct alluvial regimes based on the grain size distribution of the sediment supply: an 'active' fine-bed regime in which the slope is set by the total sediment supply, and a 'threshold' coarse-bed regime in which the slope is controlled by the threshold of motion for the coarsest grain size supplied in amounts sufficient to form a channel-spanning deposit. Early efforts to model landscape evolution (e.g. Willgoose et al., 1991; Beaumont et al., 1992) treated channel incision and slope adjustment as an essentially alluvial process. In contrast, fluvial incision and slope adjustment are represented in the current generation of landscape evolution models (e.g. Howard, 1994; Moglen and Bras, 1995; Tucker and Slingerland, 1996; Willett, 1999; Bogaart et al., 2003) as controlled primarily by the rate of bedrock detachment, rather than by the divergence of sediment transport. The rate of river incision into bedrock is commonly assumed to scale with a flow intensity parameter, such as unit stream power, average boundary shear stress, or the boundary shear stress in excess of a detachment threshold. For these 'detachment limited' models, the dominant influences on predicted channel slope are rock resistance, drainage area (a surrogate for discharge), and rates and spatial patterns of rock uplift, rather than sediment supply or grain size characteristics.

Sediment supply and grain size should strongly influence rates of bedrock incision, however, as we have recently shown through both experimental (Sklar and Dietrich, 2001) and theoretical (Sklar and Dietrich, 1998; Sklar and Dietrich, 2004) studies. In particular, sediment supplies tools that abrade exposed bedrock, but which can also inhibit incision by forming transient deposits that limit the extent of bedrock exposure in the channel bed. Moreover, grain size strongly influences the erosional efficiency of individual abrasive impacts as well as the minimum shear stress needed to prevent complete alluviation of the channel bed. Thus, the controls on the slope of a channel actively incising into bedrock are likely to include elements drawn from alluvial models (sediment supply, grain size and transport capacity) as well as from detachment-limited models (rock strength, flow intensity, tectonic boundary conditions).

Here we explore the controls on bedrock channel slope using a mechanistic model for river incision into bedrock by saltating bedload (Sklar and Dietrich, 2004), in which the dynamics of bedload sediment transport and bedrock detachment by abrasion are directly coupled. We address three distinct issues that arise in considering the implications of the 'saltation–abrasion' model for river longitudinal form.

We begin with the challenge of scaling up a model that was derived at the temporal and spatial scale of individual bedload saltation events to the scale at which landscapes evolve. In particular, we develop a new method for determining the magnitude and frequency of the discharge and sediment supply that can represent the integrated effect of the full distribution of flow events that are responsible for eroding bedrock over geomorphic time. Next we compare the saltation–abrasion model with other proposed bedrock incision models, to illustrate the importance of representing the effects of sediment supply and grain size explicitly, and to evaluate the extent to which other models capture those effects. Finally, we consider the implications of the saltation–abrasion model for understanding what controls the slope of a river channel for the limited but illustrative case when the landscape is in topographic steady state. In particular, we contrast the predictions of several models for the variation in steady-state channel slope with rock uplift rate, rock strength, and the magnitude and duration of the representative erosive flow event. Because profile relief and concavity are directly related to the integral and derivative of local channel slope with downstream distance, this analysis provides a foundation for understanding the implications of the model for longitudinal profile form.

1.2. Model overview

The saltation–abrasion model is based on the idea that incision rate can be treated as the product of three terms: the average volume of rock removed by an individual bedload impact, the impact rate per unit time per unit bed area, and the fraction of the bed not armored by transient deposits of alluvium (Sklar and Dietrich, 1998). We used several fundamental theoretical and experimental findings to derive expressions for each of these terms, including: (1) wear is proportional to the flux of impact kinetic energy normal to the bed; (2) bedload saltation trajectories can be represented as power functions of non-dimensional excess shear stress; (3) rock resistance to bedload abrasion scales with the square of rock tensile strength; and (4) the assumption

that bed cover depends linearly on the ratio of sediment supply to sediment transport capacity (Sklar and Dietrich, 2004). The predicted instantaneous rate of bedrock incision E_i can be expressed as

$$E_i = \frac{0.08 R_b g Y}{k_v \sigma_T^2} Q_s \left(\frac{\tau^*}{\tau_c^*} - 1\right)^{-1/2} \left(1 - \frac{Q_s}{Q_c}\right) \times \left(1 - \left(\frac{u^*}{w_f}\right)^2\right)^{3/2} \quad (1)$$

where R_b is the non-dimensional buoyant density $[R_b = (\rho_s - \rho_w)/\rho_w]$, g is the gravitational acceleration, Y is the rock modulus of elasticity, σ_T is the rock tensile strength, k_v is a non-dimensional rock resistance parameter (experiments indicate that $k_v \sim 10^6$, which is equivalent to 10^{12} J m^{-3} MPa^{-1}, Sklar and Dietrich, 2004), u^* is the shear velocity $[u^* = (gR_hS)^{1/2}]$, w_f is the grain fall velocity in still water (calculated here using the algorithm of Dietrich, 1982), and Q_s is the mass sediment supply rate (all variables in S.I. units). In Eq. (1), τ^* is the non-dimensional shear stress

$$\tau^* = R_h S / R_b D_s \quad (2)$$

where R_h is the hydraulic radius, S is the channel slope, D_s is the representative sediment grain diameter, and τ_c^* is the value of τ^* at the threshold of sediment motion. Hydraulic radius is solved for iteratively, assuming a rectangular channel cross-section $[R_h = H_w W/(2H_w + W)]$, using the continuity equation $[Q_w = U_w H_w W]$ and the Manning roughness relation

$$U_w = \frac{R_h^{2/3} S^{1/2}}{n_m} \quad (3)$$

where H_w is flow depth, U_w is mean flow velocity, W is channel width and n_m is the Mannings roughness parameter. Bedload sediment transport capacity Q_c is calculated here using the Fernandez-Luque and van Beek (1976) expression

$$Q_c = 5.7 \rho_s W (R_b g D_s^3)^{1/2} (\tau^* - \tau_c^*)^{3/2}. \quad (4)$$

Note that our choice of bedload transport relation is somewhat arbitrary as many other equivalent expressions are available, however, the essential outcome of the analysis below would not be changed so long as the expression for Q_c included the nearly universal non-linear dependence of transport rate on shear stress in excess of a threshold of motion stress.

The model is unique in three important respects. First, it predicts the rate of bedrock incision by a single process, abrasion by saltating bedload, rather than lumping the effects of many possible erosional mechanisms together in a single expression. Second, because all the model parameters are independent of the model formulation, it can be calibrated using laboratory experiments so that there are no freely adjustable parameters. And third, because it is derived at the temporal and spatial scale at which the erosional process occurs, it can be scaled up in space and time explicitly, so that, for example, the role of the tradeoffs between magnitude and frequency in discharge and sediment supply can be explored systematically.

2. Model application at the landscape scale

The saltation–abrasion model (Sklar and Dietrich, 2004) was derived at the temporal and spatial scale of individual bedload impacts, and predicts an instantaneous bedrock erosion rate (E_i) for specific values of the seven input variables: channel width (W), slope (S), discharge (Q_w), coarse sediment supply rate (Q_s), representative grain size (D_s), rock strength (σ_T) and channel roughness (n_m). These values can be treated as constant at a spatial scale of a channel reach, ignoring lateral variations in shear stress, and at the temporal scale of several hours to a day. To apply the model in the field and to explore the model implications for river longitudinal profile form and dynamics, the model must be scaled up, in both time and space, by many orders of magnitude. The spatial variables can be scaled using simple relationships of downstream hydraulic geometry, while temporal scaling requires a method for integrating over the full range of discharges and sediment supply events that the channel will experience.

Although bridging the gap in scale between the mechanistic derivation and the landscape application requires the introduction of several additional parameters, the physical meaning of these parameters can be explicit. Maintaining a quantitative link to the scale of individual erosive events allows us to be mechanistically consistent and observe the limitations imposed by the fundamental scales of the problem (Dietrich and Montgomery, 1998). For example, the model assumptions are violated if the grain diameter is greater than the flow depth, or if the flow is not hydraulically rough (i.e. particle Reynolds number $Re_p = \rho_s u^* D_s/\mu < 100$).

To help ground the scaling up of the model in physical reality, we use the device of a reference site, an actively incising mixed bedrock–alluvial bedded reach of the South Fork Eel River in Northern California (Seidl and Dietrich, 1992; Howard, 1998; Sklar and Dietrich, 2004). We use gauge records of discharge,

Table 1
Reference site model input values

Drainage area (A)	112 km^2
Channel slope (S)	0.0053
Median grain diameter (D_s)	0.060 m
Channel width (W)	18.0 m
Rock tensile strength (σ_T)	7.0 MPa
Assumed long-term incision rate (E_{lt})	0.9 mm/year
Predicted instantaneous incision rate (E_i)	20 mm/year

These values approximate conditions in a gauged reach of the South Fork Eel River, Mendocino County, California. Other model parameter values held constant are listed in Sklar and Dietrich (2004), Table 3.

knowledge of rates of tectonic forcing, and measurements of channel geometry, grain size, rock strength and extent of bedrock exposure, to evaluate whether the model predictions are consistent with the field setting. The reference site is also useful as an anchor point in appreciating how widely we vary the value of input variables in the sections below where we compare various bedrock incision models and explore the controls on channel slope. Table 1 lists some of the relevant characteristics of the South Fork Eel River reference site.

2.1. Spatial scaling from reach to longitudinal profile

For modeling purposes, a river profile can be represented as a series of reaches of uniform width, slope and rock strength, each with a corresponding upstream drainage area (A). For simplicity, we treat channel roughness as constant throughout the profile, although roughness may in fact vary systematically with channel slope and grain size (e.g. Bathurst, 1993). Discharge for a given recurrence interval (Q_w) is assumed to vary with drainage area as a power function

$$Q_w = bA^p \tag{5}$$

where the exponent p captures the spatial variation in precipitation due to orographic or other effects. Channel width is assumed to vary as a power function of some geomorphically significant discharge

$$W = cQ_w^f \tag{6}$$

such that width can be parameterized in terms of drainage area

$$W = cb^f A^{pf}. \tag{7}$$

In all the calculations to follow we treat width as constant for a given drainage area, consistent with the assumption of a confined bedrock gorge with a rectangular channel cross-section, lacking any floodplain. Drainage area is parameterized as a function of distance downstream of the channel head (x)

$$A = A_o + dx^h \tag{8}$$

where A_o is the drainage area upstream of the channel head, d is a dimensional coefficient and the exponent h captures the variation in drainage area shape. Note that this formulation ignores the abrupt changes in drainage area that occur at tributary junctions.

The commonly observed downstream fining of grain size is typically treated as an exponential function (e.g. Morris and Williams, 1999), however, many field studies have found good agreement with a power law fining relation (e.g. Brush, 1961; Brierley and Hickin, 1985; Ohmori, 1991). For consistency with the other spatial scaling relations we therefore model the downstream variation in representative grain diameter of the bedload size class as a power function of downstream distance

$$D_s = D_o\left(\frac{x + x_o}{x_o}\right)^{-\alpha} \tag{9}$$

where D_o is the grain size at the channel head and x_o is the unchanneled distance from the drainage divide to the channel head. Downstream changes in lithology can be represented by continuous or abrupt variation in rock tensile strength; in all calculations below we treat rock strength as uniform along the length of the profile.

Assuming that hillslope erosion rates closely track changes in rates of incision of neighboring channels, we can express the time-averaged, or mean-annual bedload sediment supply rate (Q_{sM}) as the integral of the upstream rates of river incision

$$Q_{sM} = \rho_s F_b \int E_{lt}(A)\mathrm{d}A \tag{10a}$$

which for the simple case of uniform uplift becomes

$$Q_{sM} = \rho_s F_b E_{lt} A \tag{10b}$$

where E_{lt} is the long-term bedrock incision rate averaged over all discharge and sediment supply events

$$E_{lt} = \frac{\int E_i(t)\mathrm{d}t}{\int \mathrm{d}t} \tag{11}$$

and F_b is the fraction of the total sediment supply that is coarse enough to move as bedload. If we assume the river profile is in topographic steady state, such that the long-term bedrock incision rate is equal to the rock uplift rate ($E_{lt} = U_r$), then, for the case of uniform rock uplift

$$Q_{sM} = \rho_s F_b U_r A. \tag{12}$$

The bedload fraction of the total load (F_b) can be calculated for a given boundary shear stress, if the full grain size distribution is specified, using a criterion for the threshold of suspension, such as when the shear velocity (u^*) is equal to the fall velocity in still water (w_f) (Rouse, 1937). However, because we use a single grain diameter (D_s) to represent the size of sediment moving as bedload, F_b becomes a parameter that must be estimated, rather than calculated. Measured values of F_b, from simultaneous sampling of both bedload and suspended load, range from 0.01 to 0.5 (e.g. Leopold, 1994), although field estimates of F_b in coarse-bedded mountain channels range as high as 0.82 (Bezinge, 1987).

2.2. Representative discharge and sediment supply

Landscape evolution models typically treat bedrock incision as a continuous process, and do not account explicitly for the differing effects of individual discharge and sediment supply events. This approximation may be valid for erosional processes that do not have thresholds, but because the saltation–abrasion model is based on the dynamics of bedload sediment transport we must consider the constraint imposed by the threshold of sediment motion. For example, for the South Fork Eel River reference site, the mean-annual discharge of 4 m^3/s does not produce sufficient shear stress to mobilize the representative grain size of 0.06 m, and thus would not cause bedrock wear by the mechanism of bedload abrasion. We note that other incision mechanisms, for example hydration-fracturing of clay-rich sedimentary rocks (Stock et al., 2005), may cause bedrock detachment at flows below the threshold of sediment motion.

Ideally, to calculate a long-term incision rate, we would model a time-series of discharges or integrate over a frequency distribution of discharges so that we could account for the weighted contributions of discharges of all magnitudes. For example, Tucker and Bras (2000) used the Poisson pulse rainfall model to derive a frequency distribution of flood discharges, which they integrated to explore (separately) the sensitivity of long-term rates of sediment transport and bedrock erosion to variability in runoff. Tucker and Bras (2000) did not, however, couple sediment transport and bedrock erosion, as we do here, as thus did not encounter the problem of specifying the instantaneous sediment supply rate for conditions of excess sediment transport capacity. In actively incising, mixed bedrock–alluvial channels, sediment flux will commonly be less than the discharge-dependent potential transport capacity. The extent of under-supply, or over-capacity, should vary considerably from discharge to discharge. This is because sediment supply from hillslopes to the channel network is inherently episodic, and the frequency distribution of sediment supply events, such as landslides, debris-flows and bank failures, should be to some extent decoupled from the distribution of rainfall and runoff events.

Here we use the representative discharge concept to develop a rational method for treating incision as a semi-continuous process while accounting for the effect of the threshold of sediment motion. The representative discharge is a single-value flow rate of limited duration, which we assume to represent the integrated effect of the full distribution of discharges. For consideration of the effects of sediment on bedrock incision, the method also must specify a corresponding representative sediment supply rate, which we also assume represents the integrated effect of the full distribution of sediment supply events. Here we seek to develop a simple method, with a limited number of parameters, that: (1) can be constrained by measured discharge distributions to reflect differing rainfall and runoff variability across climatic regimes; (2) accounts for the total volume of runoff, not just flood flows; (3) accounts for the total coarse sediment supply that will move as bedload rather than as suspended load; and (4) accounts for the influence of grain size on the threshold of sediment motion and thus on the bedload sediment transport capacity of the representative discharge.

In the analysis that follows, we begin by arguing for the use of two representative discharges, a high (flood) flow, and a low (base) flow, each with a specific partial annual duration, rather than a single intermittent representative discharge. We then show that a cumulative discharge distribution can be used to relate the relative magnitudes and durations of the high and low representative discharges. Next we consider the effects of the threshold of sediment motion and the non-linearity of the dependence of bedload sediment transport capacity on the representative discharge, to find an optimal partitioning of cumulative runoff between the high and low flow representative discharges. The result is a determination of the mean annual duration and magnitude of the representative high flow discharge, and the associated sediment supply rate, which are responsible for bedrock incision by bedload abrasion. Importantly, the representative sediment supply rate will be less than the sediment transport capacity of the representative high flow, consistent with the assumption of the saltation–abrasion model that excess transport capacity is required for

bedrock to be exposed in the channel bed and thus subject to abrasion.

2.3. Magnitude–frequency model development

A simple approach to constraining the magnitude of the representative discharge would be to assume that the total mean annual runoff was carried by a single representative discharge (Q_{wT}), such that

$$Q_{wT} = Q_{wM}/F_t \tag{13}$$

where Q_{wM} is the mean annual discharge and F_t is an intermittency parameter equal to the fraction of total time during which the representative discharge is assumed to occur. In the simplest case, $F_t=1$ and the mean annual discharge is assumed to represent the full discharge distribution (e.g. Tomkin et al., 2003). As noted above, in many channels the mean annual discharge will be insufficient to mobilize the bed sediments, and will therefore be a poor choice for a representative discharge for estimating long-term bedrock incision rates. For the general case of $F_t<1$ (e.g. Tucker and Slingerland, 1997), the use of Eq. (13) may exaggerate the effects of extreme events because it neglects the fraction of annual runoff that occurs in low magnitude, high frequency discharges. Such low flows may account for a significant fraction of the annual runoff in coarse-bedded channels with a high threshold of motion.

To account for the potentially important contribution of low-magnitude flows, we define two characteristic discharges, a representative high flow (Q_{wH}) and residual low flow (Q_{wL}), which together account for all the annual runoff. We define a new parameter, the fraction of the total runoff carried by the high flow (F_w), such that

$$Q_{wH} = Q_{wM}F_w/F_t \tag{14}$$

and

$$Q_{wL} = Q_{wM}(1-F_w)/(1-F_t). \tag{15}$$

We assume that by definition bedload transport only occurs during the high-flow discharge so that the sediment supply during high flow is

$$Q_s = Q_{sM}/F_t. \tag{16}$$

such that no sediment is supplied during low flow, because the shear stress is below the threshold of motion.

The two magnitude–frequency parameters, F_w and F_t, are not independent, but can be related by considering a cumulative discharge distribution. Fig. 1 shows the cumulative distribution of mean daily discharge for the South Fork Eel reference site. In Fig. 1, the probability of non-exceedence (P_{ne}) for a given discharge is computed by ranking the entire discharge record in ascending order, such that

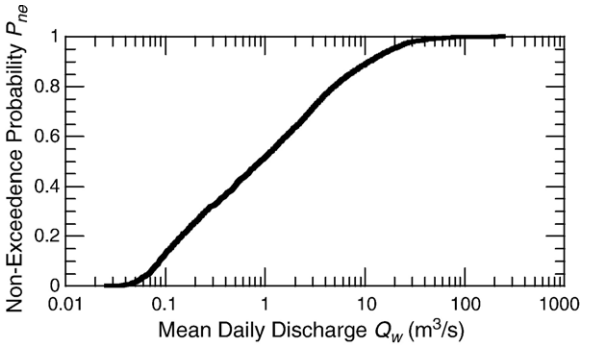

Fig. 1. Cumulative distribution of mean daily discharges from 24 year record of USGS gauge at South Fork Eel River reference site, (USGS gauge 11475500) 'near Branscom', California.

$$P_{ne} = m/(N+1) \tag{17}$$

where m is the rank of an individual discharge and N is the total number of measured discharges.

We can define the intermittency parameter F_t as

$$F_t = 1 - P_{ne} \tag{18}$$

so that the fraction of the total volume of runoff carried by the high flow F_w is

$$F_w = \frac{\int_{1-F_t}^{1} Q_w(P_{ne})P_{ne}\mathrm{d}P_{ne}}{\int_{0}^{1} Q_w(P_{ne})P_{ne}\mathrm{d}P_{ne}}. \tag{19}$$

Fig. 2a shows the relationship between F_w and F_t for the reference site gauge record. If the representative high flow is assumed to occur relatively frequently ($F_t \sim 1$) it would carry most of the annual runoff, while a less frequent, but higher magnitude representative high flow ($F_t \ll 1$) would carry only a small fraction of the annual runoff. This relationship is a way of characterizing the 'storminess' of the discharge distribution, for example the curve would shift to the left for storm dominated rivers, and to the right for spring-fed or snow-melt dominated rivers. The relationship between F_w and F_t is unlikely to be uniform within a drainage basin, for example shifting to the right with increasing distance downstream due to the integrating effect of flow routing through the channel network (Bras, 1990). Note that although we have used empirical data, this approach

could be generalized for use with synthetic discharge frequency distributions, such as the log-normal or log-Pearson distributions.

Fig. 2b shows the variation in the representative high-flow discharge (Q_{wH}) and low-flow discharge (Q_{wL}) with the high-flow time fraction (F_t), for the reference site discharge record, using Eqs. (14), (15), and (19). Also plotted in Fig. 2b is the representative discharge that carries the total runoff (Q_{wT}, Eq. (13)). As F_t declines from 1.0 (where $Q_{wH}=Q_{wT}=Q_{wM}$, and $Q_{wL}=0$), the magnitude of the high-flow discharge increases, but the rate of increase declines because of the increasing fraction of the total runoff that is carried by the low flow. In contrast, the rate of increase in total runoff representative discharge (Q_{wT}) is constant, so that for a 1 year recurrence interval (i.e. $F_t=1/365$) Q_{wT} is about an order of magnitude greater than Q_{wH}. Note that for very low values of the high flow time fraction F_t, the representative low flow is approximately equal to the mean annual discharge ($Q_{wL}\sim Q_{wM}$) and the high flow carries a negligible fraction of the annual runoff.

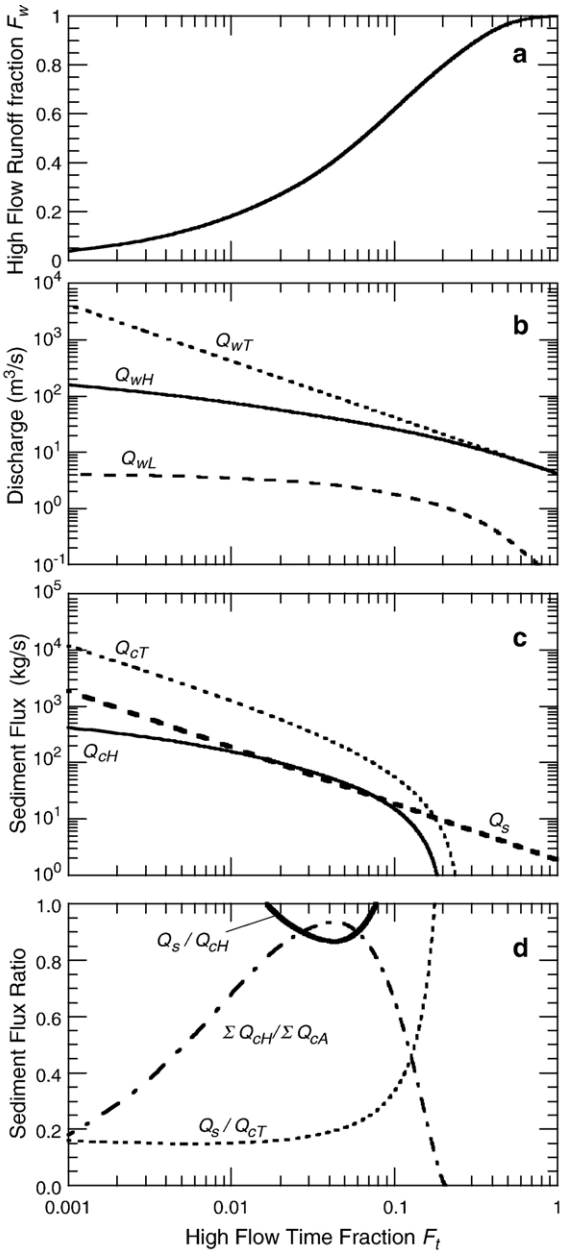

The difference between the high flow (Q_{wH}) and total flow (Q_{wT}) representative discharges is most significant when we consider sediment transport. For each discharge, we can calculate a corresponding sediment transport capacity (Q_c, Eq. (4)). Fig. 2c shows the bedload sediment transport capacity at the South Fork Eel reference site (Table 1) calculated for the high-flow (Q_{cH}) and total-runoff (Q_{cT}) representative discharge methods. Also shown is the representative sediment supply rate (Q_s), which is inversely proportional to the high flow time fraction (F_t) because we assume that all coarse sediment is moved only during high flows (Eq. (16)). For $F_t\sim 1$, the average boundary shear stress is below the threshold of motion and the transport capacity is zero. With decreasing F_t (i.e. higher magnitude, lower frequency), once the threshold of motion is exceeded the non-linearity of the sediment transport relation leads to a rapid increase in transport capacity for both the high-flow and total-runoff methods. Transport capacity (Eq. (4)) exceeds sediment supply (Eq. (16)) when $F_t<0.2$ (i.e. <70 days/year) for the total-runoff method and when $F_t<0.08$ (i.e. <29 days/year) for the high-flow method. For further decreases in F_t, the extent of excess

Fig. 2. Determination of a model high-flow discharge that best represents the integrated effect of the full distribution of discharge and sediment supply events on bedload transport and river incision into bedrock. (a) Fraction of total runoff carried by representative high flow discharge as a function of the fraction of total time that high flow occurs. (b) Variation in representative discharge with high flow time fraction for two formulations, a single discharge that carries the total annual runoff (Q_{wT}), and a pair of low-flow (Q_{wL}) and high-flow (Q_{wH}) discharges between which total annual runoff is partitioned. (c) Variation with high flow time fraction, for the total runoff formulation, of sediment transport capacity (Q_{cT}), and for the high flow formulation, sediment transport capacity (Q_{cH}) and sediment supply (Q_s), assuming all bedload transport occurs during the representative high-flow discharge. (d) Variation with high flow time fraction of: the ratio of sediment supply (Q_s) to high flow transport capacity (Q_{cH}), assumed equivalent to the extent of bedrock exposure; the ratio of the net annual high flow transport capacity to the net annual transport capacity integrated over the full gauged discharge distribution, which peaks closest to unity at $F_t=0.0437$; and the ratio of sediment supply to the transport capacity of the representative discharge using the total runoff formulation (Q_{cT}).

sediment transport capacities predicted by the two methods diverge significantly. The high flow transport capacity (Q_{cH}) only exceeds the sediment supply for a narrow range of F_t ($0.016 \le F_t \le 0.08$), while the total runoff transport capacity exceeds sediment supply for all $F_t < 0.2$.

Fig. 2d shows the ratio of sediment supply to transport capacity (Q_s / Q_c), which in the saltation–abrasion model corresponds to the fraction of the bed covered with alluvium, for the high-flow discharge (Q_s/Q_{cH}) and the total-discharge (Q_s/Q_{cT}), for reference site conditions. The high-flow method predicts only a limited extent of bedrock exposure, at an optimum F_t, while the total-runoff method predicts very large bedrock exposure over a wide range of F_t.

Because the representative discharge approach is intended to approximate the long-term net effect of the full distribution of discharges, we can use the time integral of the sediment transport capacity of the gauged discharges at the reference site as a metric to evaluate the efficacy of the two representative discharge methods. Over the 24-year period of record, the annual mean integrated bedload transport capacity ($\sum Q_{cA}$), for reference conditions, is 7.26×10^7 kg/year. Plotted in Fig. 2d is the ratio of the high flow annual transport capacity to the annual capacity of the gauged discharges ($\sum Q_{cH} / \sum Q_{cA}$), calculated over the range of F_t.

The high flow representative discharge method approximates the net sediment transport capacity of the actual discharge record best at the optimum F_t value of 0.0437 (i.e. ~16 days/year), differing only by about 5%. In contrast, the total runoff method annual net sediment transport capacity (not plotted) exceeds the actual integrated mean capacity by a factor of 2 at $F_t \sim 0.2$, and grows rapidly to a ratio of greater than 95 at $F_t = 0.0437$, and greater than 5000 by $F_t = 0.001$.

The preceding analysis provides a rational procedure for assigning values to the magnitude–frequency scaling parameters; for the reference site we find an optimal value for the high flow time fraction of $F_t = 0.0437$, which corresponds to a high flow runoff fraction of $F_w = 0.41$. The result that nearly 60% of the annual discharge is carried by the representative low-flow discharge shows the importance of using a flow partitioning approach in generating a representative discharge for simulating bedload sediment transport as a semi-continuous process.

2.4. Field reference site calibration

We have used the discharge record and channel conditions of the South Fork Eel River reference site to describe a rational method for constraining the magnitude–frequency scaling parameter F_t. We next use the reference site to constrain the value of the remaining free scaling parameter, the fraction of total load in the bedload size class F_b, so that the predicted incision rates of the calibrated saltation–abrasion model are consistent with the field conditions.

For simplicity, we assume that the reference site reach and upstream watershed are in approximate topographic steady state, with bedrock incision and landscape lowering rates equal to the local rate of rock uplift. From analysis of marine terraces, Merritts and Bull (1989) mapped the variation in rock uplift rate over a 130 km transect parallel to the Northern California coastline. For the South Fork Eel River reference site, located at about km 80 of the transect, Merritts and Bull's (1989) data (their Fig. 5) suggest a long-term average rock uplift rate of 0.9 mm/year. Assuming that bedrock incision is confined to high flows that occur 16 days/year on average ($F_t = 0.0437$), the corresponding instantaneous incision rate ($E_i = E_{lt}/F_t$) is 20 mm/year. The saltation–abrasion model predicts this incision rate if the bedload fraction F_b is set to 0.22, for the reference site drainage area, rock strength, and channel geometry (Table 1). The corresponding predicted fraction of bed cover is 0.85, roughly consistent with the mapped extent of bedrock exposure under contemporary conditions.

These calculations illustrate how the saltation–abrasion model, which was derived at the scale of individual particle impacts can be scaled up in time and space to apply at the scale of landscape adjustment to rates of rock uplift. The scaling parameters (F_t, F_w, and F_b) are constrained by the gauged discharge record and by estimates of the regional rock uplift field, to occupy a limited range of physically reasonable values. In combination with the experimental calibration of the rock strength parameter k_v, the reference site calibration demonstrates that the saltation–abrasion model is physically consistent with both the dynamics of individual bedload grain impacts on an exposed bedrock bed, and the long-term evolution of river channels in response to climatic and tectonic forcing.

3. Contrasts with other bedrock incision models

Although many other bedrock incision models have been proposed, none account fully for the effects of sediment that emerge from a mechanistic consideration of the coupling of bedload sediment transport and bedrock wear by bedload particle impacts. In this section we use the saltation–abrasion model as a

reference model to evaluate how other bedrock incision models treat the effects of sediment, and explore the relative importance of explicitly representing each of these effects. Despite the importance of bedrock incision rules for the outcomes of landscape evolution simulations, few studies have systematically compared the behavior of multiple incision models. Tucker and Whipple (2002) contrasted the topographic outcomes of several incision models, some of which explicitly represented sediment supply, however, none of the models included the effects of grain size. Similarly, van der Beek and Bishop (2003) and Tomkin et al. (2003) tested the ability of various incision models to simulate the evolution of specific river longitudinal profiles, however, the effects of grain size were also not included in any of the models investigated.

Sediment supply and grain size introduce four distinct effects: the tools and cover effects, and the constraints imposed by the thresholds of motion and suspension. The tools effect arises because there must be some coarse sediment supplied for there to be tools available to abrade the bed. The cover effect refers to the assumption that the sediment supply rate must be less than the sediment transport capacity for some bedrock to be exposed in the channel bed, and thus subject to impacts by saltating bedload. The threshold of motion, which is determined by grain size for a given shear stress, must be exceeded for abrasion by mobile sediment to occur. Finally, particle motion must be below the threshold of suspension, also determined by grain size for a given flow intensity, for abrasion by bedload motion to occur. Note that the saltation–abrasion model only applies to bedload; abrasion by suspended grains and all other incision mechanisms are not considered here. Note, however, that the cover effect should inhibit all bedrock detachment mechanisms, with the possible exception of dissolution.

3.1. Model classification

Bedrock incision models can be grouped according to which, if any, of the effects of sediment are explicitly represented. Three of the four sediment effects have been recognized to some extent in previous models, the tools effect, the cover effect, and the threshold of motion. The fourth effect, the threshold of suspension, is introduced in the saltation–abrasion model because bedload impacts are the only erosional mechanism considered. Below we review model formulations that encompass the range of possible combinations of sediment effects, including some that have not been previously proposed, in order to clearly demonstrate the implications of each of the sediment effects for predictions of bedrock incision rates.

We begin by defining a generic bedrock incision expression that can be used as a common basis for comparing different models. Each of the published bedrock incision models that we are aware of can be expressed in a form based on Eq. (1)

$$E_i = K_\gamma \gamma^a Q_s^b \left(1 - \frac{Q_s}{Q_t}\right)^c \left[1 - \left(\frac{u^*}{w_f}\right)^2\right]^d \tag{20}$$

where γ is a placeholder variable for the various model measures of flow intensity (e.g. stream power), and the coefficient K_γ is a placeholder erosional efficiency coefficient that represents rock strength and other factors. The tools effect, cover effect and threshold of suspension are controlled by the exponents b, c, and d respectively, and the threshold of motion effect is expressed in the choice of γ and in the choice of sediment transport capacity relation for Q_c. Table 2 summarizes the parameterization of each model formulation in terms of the variables, coefficient and exponents of Eq. (20). Note that for each model formulation the value of K_γ is tuned to match the assumed representative conditions and incision rate of the S. Fork Eel River reference site.

3.1.1. Class I: no sediment effects

The most widely used bedrock incision models do not explicitly account for any of the possible effects of sediment. These include the stream power model (Seidl and Dietrich, 1992)

$$E = K_\Omega \Omega^n \tag{21}$$

the unit stream power model (Howard et al., 1994)

$$E = K_\omega \omega^n \tag{22}$$

and the shear stress model (Howard and Kerby, 1983)

$$E = K_\tau \tau^n \tag{23}$$

where $\Omega = \rho_w g Q_w S$ is the stream power per unit downstream length, $\omega = \rho_w g Q_w S / W$ is the stream power per unit bed area, $\tau = \rho_w g R_h S$ is the force per unit area exerted by the flow averaged over the channel boundary, and K_Ω, K_ω and K_τ are proportionality constants intended to represent implicitly the effects of rock resistance and many other factors, including sediment (Howard et al., 1994; Sklar and Dietrich, 1998; Whipple and Tucker, 1999). Eqs. (21), (22) and (23) are equivalent to Eq. (20) with $a = n$ and $b = c = d = 0$.

Table 2
Incision model comparison: classification, Eq. (19) model parameters and reference site parameterization

Class	Equation	Model	γ	a	b	c	d	Kγ (for reference site)	Original citation
I	21	Unit Stream Power [SP]	ω	1	0	0	0	0.18 (mm/year)/ (W/m^2)	Seidl and Dietrich, 1992
I	22	Shear Stress [SS]	τ	1	0	0	0	0.41 (mm/year)/Pa	Howard and Kerby, 1983
I	23	Excess Shear Stress (rock) [ESS-rock]	$\tau-\tau_c$ (rock)	1	0	0	0	0.20 (mm/year)/Pa	Howard, 1994
I		Dimensionless Shear Stress	τ^*	1	0	0	0	400 mm/year	Lavé and Avouac, 2000
II	24	Excess Shear Stress (sediment) [ESS-sed]	$\tau-\tau_c$ (sed)	1	0	0	0	1.0 (mm/year)/Pa	This study
II		Dimensionless Excess Shear Stress	τ^*/τ_c^*	1	0	0	0	962 mm/year	This study
II		Alt Dimensionless Excess Shear Stress	τ^*/τ_c^*-1	1	0	0	0	28.9 mm/year	This study
III	26	Modified-Alluvial (n=1) [MA(1)]	ω	1	0	1	0	2.7 (mm/year)/ (W/m^2)	Beaumont et al., 1992
III	26	Modified-Alluvial (n=2) [MA(2)]	ω	2	0	1	0	0.0106 (mm/year)/ (W^2/m^4)	Whipple and Tucker, 2002
IV	27	Modified-Alluvial (Bedload) [MA(bdld)]	τ^*/τ_c^*-1	1.5	0	1	0	225 (mm/year)/ (kg/s)	This study
V	28	Tools [Tools]	$\tau*/\tau_c^*-1$	−0.5	1	0	0	0.405 (mm/year)/ (kg/s)	Foley, 1980; this study
VI	30	Parabolic Stream Power (n=1) [SPP(1)]	ω	0	1	1	0	0.353 (mm/year)/ (W/m^2)	Whipple and Tucker, 2002
VI	30	Parabolic Stream Power (n=2) [SPP(2)]	ω	1	1	1	0	0.003 (mm/year)/ (w^2/m^4)	Whipple and Tucker, 2002
VII	1	Saltation–abrasion (no suspension)	τ^*/τ_c^*-1	−0.5	1	1	0	2.70 (mm/year)/ (kg/s)	Sklar and Dietrich, 2004
VIII	1	Saltation–abrasion [SA]	$\tau*/\tau_c^*-1$	−0.5	1	1	1	2.70 (mm/year)/ (kg/s)	Sklar and Dietrich, 2004

Considerable debate has surrounded the choice of n and γ, with $n=1$ most commonly used (e.g. Tucker and Slingerland, 1994; Willett, 1999) although Whipple et al. (2000) argue for values of n ranging between 2/3 and 5/3 depending on the dominant incision mechanism.

The excess shear stress model (Howard et al., 1994; Tucker and Slingerland, 1997)

$$E = K_{\tau-\mathrm{cr}}(\tau - \tau_{\mathrm{c-rock}})^n \tag{24}$$

accounts for the possibility that incision only occurs when shear stress exceeds a critical value $\tau_{\mathrm{c\text{-}rock}}$ below which no bedrock wear occurs. A similar model could be formulated with incision proportional to stream power in excess of a threshold. The threshold shear stress $\tau_{\mathrm{c\text{-}rock}}$ is assumed to be a property of bedrock strength, with higher values for more resistant lithologies. No data are available to guide parameterization of this threshold, although Whipple et al. (2000) discuss the threshold behavior of rock erosion by the mechanism of plucking. It is important to note that no detachment threshold was observed in the bedrock abrasion mill experiments of Sklar and Dietrich (2001) in which bedload abrasion was the dominant erosional mechanism. A similar detachment threshold for cohesive hillslope materials is a key parameter in mechanistic theories for channel initiation (e.g. Montgomery and Dietrich, 1988, 1992), and has been used in numerical simulations of landscape evolution focused on drainage density (Tucker and Bras, 1998).

3.1.2. Class II: grain size effects only

The excess shear stress model can alternatively be defined to incorporate the threshold of sediment motion

$$E = K_{\tau-\mathrm{cs}}(\tau - \tau_{\mathrm{c-sed}})^n \tag{25}$$

where $\tau_{\mathrm{c\text{-}sed}}$ is the shear stress required to mobilize non-cohesive bed sediments and is a generally a linear function of grain size (Buffington and Montgomery, 1997). This represents a second class of incision models in which grain size must be specified but the tools, cover and suspension effects are neglected. The magnitude of $\tau_{\mathrm{c\text{-}rock}}$ should be significantly greater than $\tau_{\mathrm{c\text{-}sed}}$ because of the cohesive nature of rock; for purposes of model comparison we arbitrarily set $\tau_{\mathrm{c\text{-}rock}}$ to be five times

greater than $\tau_{c\text{-}sed}$ for the reference site grain diameter of 0.06 m. The sediment-based excess shear stress model can equivalently be expressed in non-dimensional form with $\gamma=\tau^*-\tau_c^*$ or $\gamma=\tau^*/\tau_c^*-1$. Like the stream power and shear stress models, the various formulations of the excess shear stress model are represented by Eq. (20) with $a=n$ and $b=c=d=0$.

Another model that requires specification of the sediment grain size was proposed by Lave and Avouac (2001). It is a modified form of the shear stress model (Eq. (23)) in which the flow intensity variable $\gamma=\tau^*$ and $n=1$. Although this approach does explicitly include grain size, it does not account for the non-linear effect introduced by the size-dependent threshold of grain motion.

3.1.3. Class III: sediment supply effects only

The simplest approach to including the effect of sediment supply is to treat bedrock incision rate as proportional to the sediment transport capacity in excess of the supply

$$E = K_{ma}(Q_c - Q_s) = K_{ma}Q_c(1 - Q_s/Q_c) \tag{26}$$

where $Q_c=f(\gamma)$ and K_{ma} is an erosional efficiency constant, as first proposed by Beaumont et al. (1992). Eq. (26) represents a third class of incision models, which capture the coverage effect but not the tools effect nor the grain size dependent effects of the thresholds of motion and suspension. Although the term 'under-capacity' is often used, we refer to models of this type as 'modified alluvial' because they differ from alluvial incision models only in the value of the parameter K_{ma}. If $K_{ma}=1/\rho_s(1-\lambda)WL_r$, where λ is bed porosity and L_r is a characteristic reach length, then Eq. (26) is simply the conservation of mass equation for a channel with an infinitely thick alluvial mantle. In landscape evolution simulations K_{ma} is typically set to a much lower value, however, to account for the cohesive properties of bedrock (e.g. Kooi and Beaumont, 1996). In the framework of Eq. (20), $c=1$, $b=d=0$, and a and γ depend on the choice of sediment transport relation. Two variations of the modified-alluvial model have been proposed, which assuming that sediment transport capacity is proportional to stream power (i.e. $Q_c=K_{qa}\omega$), can be written as

$$E = K_n\omega^n(1 - Q_s/K_{qa}\omega) \tag{27}$$

where $n=1$ (Beaumont et al., 1992) or $n=2$ (Whipple and Tucker, 2002), and $a=n$ in Eq. (20).

Note that the modified-alluvial model is commonly motivated by the argument that sediment supply inhibits incision by extracting energy from the flow for sediment transport, energy that would otherwise be available for incision of bedrock (Beaumont et al., 1992). However, as we argued in developing the saltation–abrasion model (Sklar and Dietrich, 2004), it is precisely because energy is transferred from the flow to the sediment that bedrock erosion occurs, at least for the mechanism of abrasion. The coverage effect arises because grain interactions inhibit energy transfer from the mobile sediment to the bedrock. Although this is a subtle distinction, it may account for the omission of a tools effect term in landscape evolution models using the modified-alluvial incision rule.

3.1.4. Class IV: sediment supply and grain size effects only

If we use a bedload sediment transport relation in the modified alluvial model, we obtain a fourth class of incision model, which, in addition to accounting for the coverage effect, explicitly includes the threshold of motion and scales flow intensity by grain size. Combining Eqs. (4) and (26) we obtain

$$E = K_{ma\text{-}b}\left[5.7\rho_s W(R_b g D_s^3)^{1/2}(\tau_c^*)^{3/2} \times \left(\frac{\tau^*}{\tau_c^*}-1\right)^{3/2} - Q_s\right] \tag{28}$$

which can be parameterized in Eq. (20) with $\gamma=\tau^*/\tau_c^*-1$, $a=1.5$, and $b=1.0$.

3.1.5. Class V: grain size and tools effects only

Foley's (1980) pioneering mechanistic incision model represents a fifth class of possible incision models, those which include the tools effect and threshold of motion, but not the coverage effect and threshold of suspension. This model, which applies Bitter's (1963) impact wear theory to the saltating motion of an individual grain without accounting for grain interaction, can be expressed as

$$E = \frac{K_f w_{si}^2 Q_s}{L_s W}. \tag{29}$$

Eq. (29) is equivalent to Eq. (20) with $b=1$ and $c=d=0$. Unfortunately, Foley (1980) did not specify the functional relationships $L_s=f(\gamma)$ and $w_{si}=f(\gamma)$, however, we can use the empirical saltation trajectory relations developed previously (Sklar and Dietrich, 2004; Eqs. (27) and (34)) to obtain $\gamma=\tau^*/\tau_c^*-1$ and $a=-0.5$. Another version of the tools-based model was proposed by Howard et al. (1994) who used data from Head and

Harr (1970) and Wiberg and Smith (1985) to parameterize Foley's (1980) model as

$$E = K_h(Q_s/W)(Q_w/W)^{0.5}S^{0.4}D_s^{-0.1} \quad (30)$$

for $\tau^*/\tau_c^* > 1.3$; this is approximately equivalent to $\gamma = \omega$ and $a = 0.45$ in Eq. (20).

3.1.6. Class VI: cover and tools effects only

A sixth class of bedrock incision models account for both the tools and coverage effects but neglect the thresholds of motion and suspension. For example, Whipple and Tucker (2002), responding to our earlier findings (Sklar and Dietrich, 1998), proposed a parabolic modification of the unit stream power model (Eq. (22)) that can be written as

$$E = K_\omega \omega^n [1 - 4(Q_s/Q_t - 0.5)^2] = K_p \omega^{n-1} Q_s (1 - Q_s/Q_t) \quad (31)$$

for $Q_c = K_{qa}\omega$ and $K_p = 4K_\omega/K_{qa}$. The parabolic model of Eq. (31) is equivalent to Eq. (20) with $b = c = 1$, $d = 0$ and $a = n - 1$. Whipple and Tucker (2002) discuss the cases where $n = 1$ and $n = 2$.

3.1.7. Class VII: tools, cover and threshold of motion only

A seventh class of incision models account for the threshold of motion along with the tools and cover effects, neglecting only the effect of the threshold of suspension. This is what we would obtain with the saltation–abrasion model of Eq. (1) if we omit the saltation length extrapolation term $[1 - (u^*/w_f)^2]$, so that $a = -0.5$, $b = c = 1$ and $d = 0$ in Eq. (20). Note that this is equivalent to the linear parabolic model (Eq. (31) with $n = 1$) if $\gamma = \tau^*/\tau_c^* - 1$ rather than ω (i.e. if a bedload sediment transport relation is used).

3.1.8. Class VIII: tools, cover, threshold of motion and threshold of suspension

Finally, the full saltation–abrasion model (Eq. (1)) constitutes an eighth model class, in which each of the four principal effects of sediment are explicitly accounted for.

3.2. Model comparisons

In this section we compare the incision rates predicted by the various models defined above, for variations in sediment supply rate and transport stage (τ^*/τ_c^*). As noted above, the coefficients of each of the models are tuned to predict the assumed long-term incision rate at the South Fork Eel reference site. This creates a common benchmark erosion rate, so that we can compare predicted deviations from that erosion rate as we vary sediment supply and transport stage.

Fig. 3 shows incision rate as a function of sediment supply, holding all other variables, such as shear stress, grain size, and rock strength, constant at reference site values. The reference site is indicated by the open circle. Four types of behavior can be seen. In the trivial case, models with no sediment supply effects (Classes I and II) plot as a horizontal line because predicted incision rate is independent of sediment supply. Models that account for the cover effect, but not the tools effect (Classes III and IV) predict a linear decrease in incision rate with increasing sediment supply, becoming zero when the sediment supply equals the transport capacity; maximum incision rates occur when sediment supply is minimized. Conversely, tools-based models (Class V) predict a linear increase in incision rate with increasing sediment supply; incision rate is maximized when sediment supply is greatest. The saltation–abrasion model, and the other models that account for both the cover and tools effects (Classes VI, VII and VIII) predict a parabolic dependence of incision rate on sediment supply, in which the peak incision rate occurs at a moderate sediment supply rate.

To compare model predictions of incision rate as a function of transport stage, it is convenient to use a three-dimensional depiction of the incision model

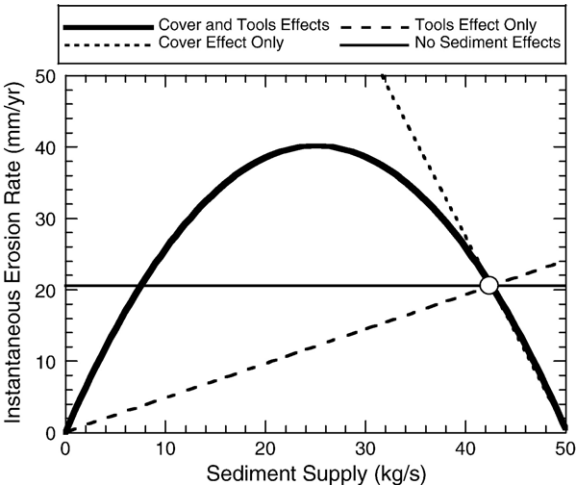

Fig. 3. Instantaneous bedrock erosion rate as a function of sediment supply for four classes of incision models that each account for different sets of effects of sediment, calculated holding all other variables constant at South Fork Eel River references site conditions. Open circle indicates the instantaneous incision rate that corresponds to the assumed long term bedrock erosion rate at the reference site, for $F_t = 0.0437$.

functional surface, as we have done previously (Sklar and Dietrich, 2004). As shown in Fig. 4, each incision model can be represented fully by plotting contours of constant incision rate (axis out of the page) as functions of transport stage and the ratio of sediment supply to sediment transport capacity (Q_s/Q_c; also referred to as relative sediment supply). Note that the contour spacing is logarithmic to encompass incision rates ranging over many orders of magnitude. Note also that transport stage occurs on the relative sediment supply axis as well, because sediment transport capacity is a non-linear function of transport stage (Eq. (4)).

Depicting the incision functions in this format allows the principal effects of sediment to occur along discrete axes. The thresholds of motion and suspension are expressed along the transport stage axis, while the cover and tools effect are expressed along the relative supply axis. As we have shown previously (Sklar and Dietrich,

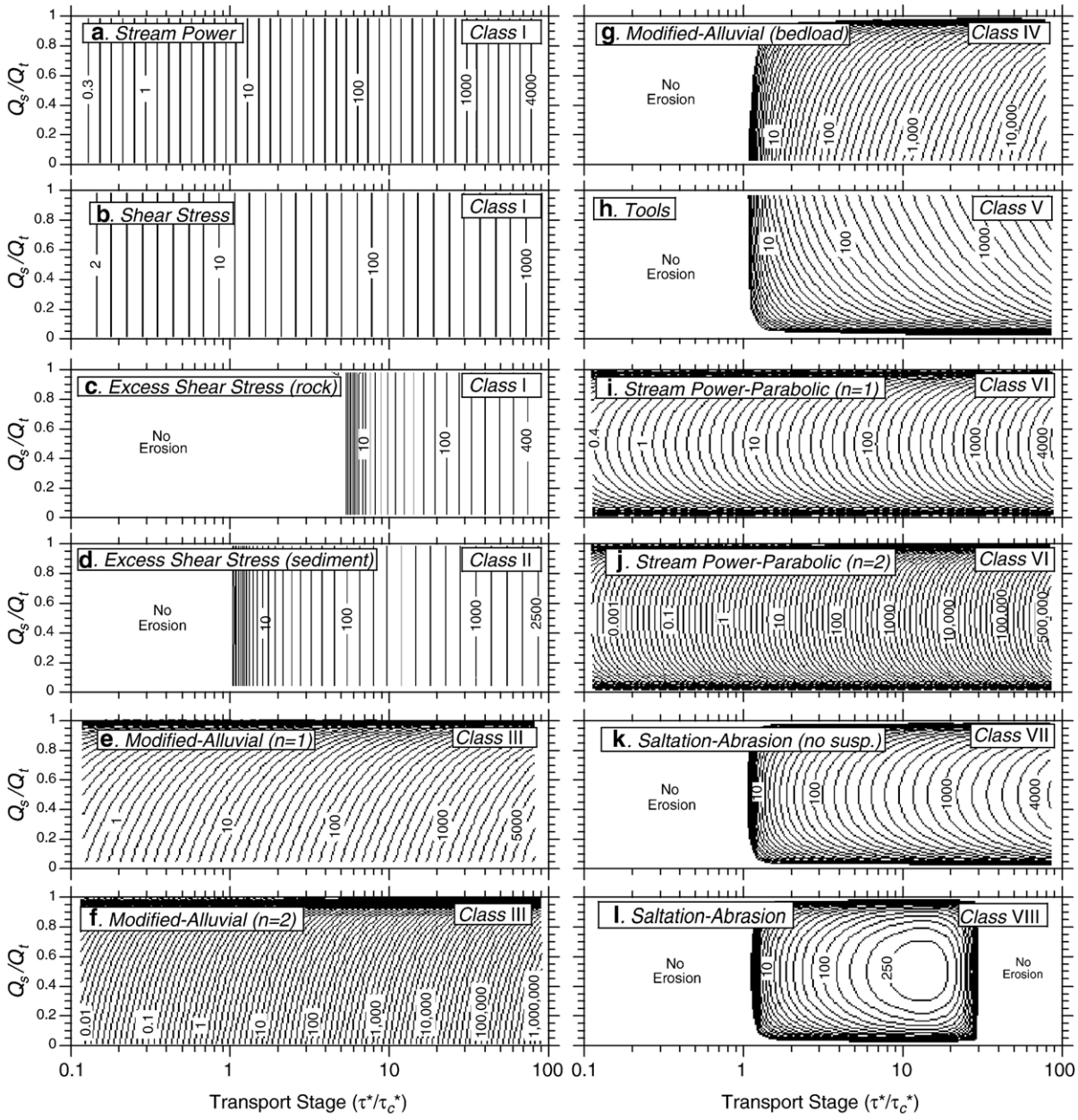

Fig. 4. Bedrock incision rate (mm/year) predicted by various models (contours, axis out of the page, logarithmic spacing) as a function of transport stage and relative sediment supply (Q_s/Q_c), for reference site values of grain size (D_s=0.06 m) and rock tensile strength (σ_T=7.0 MPa).

2004), when incision rate is non-dimensionalized by rock strength and grain size, the saltation–abrasion model plots in this parameter space as a unique surface, valid for all physically reasonable combinations of discharge, slope, width, sediment supply, grain size, rock strength and channel roughness. For model comparison purposes we have used the dimensional instantaneous incision rate E_i (mm/year), with model parameters tuned to match the reference site incision rate (Table 1).

The fundamental differences between the incision model classes are clearly apparent in Fig. 4. Models with no sediment effects plot as simple inclined planes (Fig. 4a and b), with the sensitivity to shear stress expressed by the density of contour lines. Models that require a shear stress in excess of a threshold for incision to occur, either a rock strength-dependent detachment threshold (Fig. 4c) or the threshold of motion (Fig. 4d, g, j, k and l), have a zone of 'no erosion' for stresses below the threshold. Where the cover effect is accounted for (Fig. 4e, f, g, i, j, k, l), incision rate contours curve to the right as the threshold of alluviation is approached ($Q_s/Q_c \sim 1$) and incision rate goes to zero. Similarly, where the tools affect is accounted for (Fig. 4h, i, j, k and l), incision rate contours curve to the right as sediment supply, and thus the incision rate, approach zero. Because the saltation–abrasion model also accounts for the threshold of suspension, there is also a zone of 'no erosion' for shear stresses above this threshold (Fig. 4l). Due to the suspension effect, the saltation–abrasion model predicts that there is a limit to the potential rate of bedrock wear by bedload abrasion, for all possible values of transport stage and sediment supply, as indicated by the peak of the incision function surface (Fig. 4l). All other models considered here, which in principle are intended to represent incision by multiple erosional mechanisms, predict continuously increasing incision rates with increasing transport stage.

Comparison of Figs. 3 and 4 shows that the curves of incision rate as a function of sediment supply, plotted in Fig. 3, are simply slices through the functional surfaces plotted in Fig. 4, parallel to the relative sediment supply axis. A similar slice through the functional surfaces can be made parallel to the transport stage axis, in order to depict the dependence of incision rate on transport stage, independent of the influence of transport stage on the sediment transport capacity. Fig. 5 shows slices through each of the functional surfaces of Fig. 4, along a line of constant relative sediment supply ($Q_s/Q_c = 0.5$).

Three fundamental differences between incision model classes are clearly illustrated in Fig. 5. First, models that do not account for the threshold of motion predict significant rates of incision when the flow

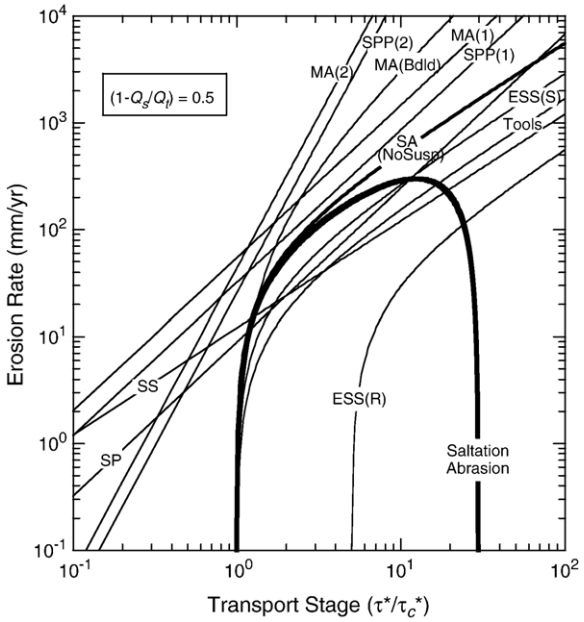

Fig. 5. Bedrock erosion rate as a function of transport stage for various incision models, for constant relative sediment supply ($Q_s/Q_c = 0.5$). Model abbreviations listed in Table 2.

intensity is too weak to move bedload. These include the stream power [SP, SP(2)], shear stress (SS), modified-alluvial [MA, MA(2)], and parabolic stream power [SPP, SPP(2)] models. Second, with the exception of saltation–abrasion [SA], all models neglect the threshold of suspension, and thus predict extremely rapid rates of incision when sediment transport is dominated by suspended load ($\tau^*/\tau_c^* > 30$), despite the probability that suspended grains collide very infrequently with the channel bed. Third, most models tend to over-predict the rate of growth of incision rate, relative to the saltation–abrasion model, even at moderate levels of transport stage. This is particularly true of the non-linear ($n = 2$) versions of the modified alluvial and parabolic stream power models. The bedload version of the modified alluvial model [MA(bdld)] also predicts very rapid growth in incision rate as transport stage increases beyond the threshold of motion. Note that the excess shear stress model with a rock strength-dependent detachment threshold [ESS(R)] plots apart from the other models in Fig. 5 because we have set the threshold shear stress to a value five times larger than the threshold of sediment motion shear stress, to account for the cohesive nature of rock.

Each incision model considered here can be tuned to be approximately equivalent to the saltation–abrasion model, over a limited range of variation in sediment supply and transport stage. For example, as shown in Fig.

3, the modified alluvial model predicts a similar variation incision rate for relatively high sediment supply rates and fixed transport stage, but vastly over predicts incision rate for low sediment supply rates, compared to the saltation–abrasion model. Similarly, each of the models that account for the threshold of motion predict similar incision rates for relatively low transport stages (for constant Q_s/Q_c; Fig. 5), but diverge rapidly as τ^*/τ_c^* increases above ~2.0. The bedload version of the modified alluvial model perhaps best approximates the saltation–abrasion model, but only for the narrow range of low transport stage ($\tau^*/\tau_c^*<3$) and high relative sediment supply ($Q_s/Q_c>0.8$). These conditions may, however, be relatively common in many mountain rivers when bedrock incision is taking place.

The fundamentally different model behaviors illustrated in Fig. 4 can be expected to correspond to large differences in predicted landscape response to changes boundary conditions, such as rock uplift rate, rock strength and discharge regime. In the following section we explore the landscape implications of including or neglecting the various effects of sediment in bedrock incision models, by considering the controls on channel slope for the case of topographic steady state.

4. Controls on steady-state channel slope

The complex role of sediment in influencing bedrock incision rates has important implications for understanding the controls on the slope of a given reach of river channel. And because river longitudinal profile relief and concavity are directly related to the integral and derivative of channel slope along the length of the profile respectively, understanding the controls on local channel slope is essential to explaining river profile form in general. For simplicity, we focus here on steady-state channel slopes. Landscapes subject to prolonged steady rock uplift may approach an equilibrium condition where erosion rate everywhere balances rock uplift rate and topography reaches a steady state (Hack, 1960). At steady state, erosion rate is determined simply by the rate of rock uplift, and channel slope becomes the dependent variable. The equilibrium slope of an incising river is then a function of the rate of rock uplift, as well as the other variables influencing the instantaneous incision rate, in particular sediment supply, grain size, discharge, and rock strength. In this section we explore the implications of the cover and tools effects and the thresholds of motion and suspension in controlling channel slope at a reach scale, and contrast the predictions of the saltation–abrasion model with the other types of models used in landscape evolution simulations.

4.1. Components of steady-state channel slope

Recognition of the constraints on bedrock incision rates imposed by the threshold of grain motion and the threshold of alluviation, suggests that a hierarchy of channel slopes exists. The minimum slope required for bedrock incision to occur is set by the threshold of motion. For a given discharge and channel geometry, if slope is not steep enough to generate shear stresses in excess of the threshold of motion, no sediment transport and no incision occur. If the slope is steep enough to mobilize bed sediments, but not steep enough to transport bedload out of the reach at the rate that coarse sediments are supplied to the reach from upstream and from adjacent hillslopes, then we assume that no bedrock will be exposed in the channel bed, incision rate will be zero, and bed aggradation will occur. For incision to occur, we assume that the slope must be steeper than the slope required to transport the imposed sediment load, in order to provide the excess transport capacity to generate sufficient bedrock exposure and bedload particle impact energy and frequency.

Therefore, steady-state total channel slope (S) can be considered to be a sum of component terms

$$S = S_{D_s} + \Delta S_{Q_s} + \Delta S_E \tag{32}$$

where S_{D_s} is the threshold of motion slope, ΔS_{Q_s} is the increment of slope above S_{D_s} required to transport sediment at the rate of supply, and ΔS_E is an additional slope increment required to erode bedrock at the rate of rock uplift. Using the bedload sediment transport relation of Eq. (4) (Fernandez-Luque and van Beek, 1976), we obtain

$$S_D = \tau_c^* R_b D_s / R_h \tag{33}$$

and

$$\Delta S_{Q_s} = \frac{R_b D_s}{R_h}\left(\frac{Q_s}{5.7\rho_s W (R_b g D_s^3)^{1/2}}\right)^{2/3} \tag{34}$$

For the saltation abrasion model, because slope occurs in both the flow intensity term and the cover term (Eq. (20); Table 2), ΔS_E cannot be solved for analytically, and instead must be solved for numerically. Below, in comparing the steady-state channel slopes predicted by the various classes of incision models, we will use the slope component framework to help understand the behavior of the saltation–abrasion model, and the deviations from this behavior of the other models.

4.2. Analytical solutions for steady-state channel slope

Analytical solutions for steady-state channel slope can be derived for the other bedrock incision models discussed in the preceding section. In order to evaluate the predicted influence of rock strength on steady-state channel slope (below), we modify the incision efficiency coefficients of each model expression to explicitly include the square of rock tensile strength (σ_T^2) as a proxy for rock resistance to wear. We have demonstrated previously (Sklar and Dietrich, 2001) that rock resistance to wear by bedload abrasion scales with σ_T^2. Here we assume for simplicity that the same scaling relationship applies to rock resistance to wear by all incisional mechanisms represented by the other model expressions. Using the unit stream power model as an example ($n=1$), we now write Eq. (22) as

$$E = K_{\omega\sigma}\rho_w g Q_w S/\sigma_T^2 W \tag{35}$$

where $K_{\omega\sigma}=K_\omega/\sigma_T^2$.

Rearranging Eq. (35) to solve for slope we obtain

$$S = E\sigma_T^2 W/K_{\omega\sigma}\rho_w g Q_w. \tag{36}$$

Similarly, for the shear stress model (Eq. (23))

$$S = \left(\frac{E\sigma_T^2}{K_{\tau\sigma}\rho_w g}\right)^{10/7}\left(\frac{W}{Q_w n}\right)^{6/7} \tag{37}$$

the excess shear stress model, with a rock detachment threshold (Eq. (24)

$$S = \left[\left(\frac{E\sigma_T^2}{K_{\tau-cr\sigma}} + \tau_{c-rock}\right)\frac{W^{3/5}}{\rho g (Q_w n)^{3/5}}\right]^{10/7} \tag{38}$$

the excess shear stress model, with a sediment motion threshold (Eq. (25))

$$S = \left[\left(\frac{E\sigma_T^2}{K_{\tau cs\sigma}} + \tau_{c-sed}\right)\frac{W^{3/5}}{\rho_w g (Q_w n)^{3/5}}\right]^{10/7} \tag{39}$$

the modified-alluvial model (Eq. (27)), with $n=1$

$$S = \left(\frac{E\sigma_T^2}{K_{a\sigma}} + Q_s\right)\frac{W}{K_{bl}\rho_w g Q_w} \tag{40}$$

and with $n=2$

$$S = \frac{Q_s W}{2K_{bl}\rho_w g Q_w}\left[1 + \left(1 + \frac{E\sigma_T^4 4K_{bl}^2}{Q_s^2 K_{a2\sigma}}\right)^{1/2}\right] \tag{41}$$

the bedload modified alluvial model (Eq. (28))

$$S = \left\{\left[\left(\frac{E\sigma_T^2 + Q_s K_{ma-b\sigma}}{5.7 K_{ma-b\sigma}\rho_s W\left(R_b g D_s^3\right)^{1.2}(\tau_c^*)^{3/2}}\right)^{2/3} + 1\right] \times \frac{R_b D_s \tau_c^*}{\left(\frac{Q_w n}{W}\right)^{3/5}}\right\} 10/7 \tag{42}$$

the tools model (Eq. (29) parameterized as Eq. (20) with b=1 and c=d=0)

$$S = \left\{\left[\left(\frac{K_{f\sigma} Q_s}{E\sigma_T^2}\right)^2 + 1\right]\frac{R_b D_s \tau_c^*}{\left(\frac{Q_w n}{W}\right)^{3/5}}\right\}^{10/7} \tag{43}$$

the parabolic stream power model (Eq. (31)), with $n=1$

$$S = \frac{Q_s W}{K_{bl}\rho_w g Q_w (1 - E\sigma_T^2 K_{bl}/4K_{\omega\sigma}Q_s)} \tag{44}$$

and with $n=2$

$$S = \frac{W}{\rho_w g Q_w}\left(\frac{K_{bl}\sigma_T^2 E}{4K_{\omega 2\sigma}Q_s} + \frac{Q_s}{K_{bl}}\right) \tag{45}$$

4.3. Comparisons of incision model predictions of steady-state channel slope

In this section we compare the steady-state channel slope predicted by the saltation–abrasion model with the slopes predicted by the other incision models discussed above. Our analysis focuses on the sensitivity of steady-state slope to variations in rock uplift rate and rock resistance to erosion, in part because the two most common incision models in landscape evolution studies, the stream power and shear stress models, predict linear variation in slope with both variables. As we demonstrate below, the saltation–abrasion model predicts a highly non-linear relationship between slope and rock uplift rate and very little dependence of slope on rock strength. To the extent that other models incorporate the various effects of sediment on incision rate, they too deviate from the linear relationships of the stream power and shear stress models.

We also evaluate the sensitivity of slope to the magnitude–frequency parameter F_t, which, as defined above, represents the fraction of time during which the high flows that transport sediment and incise bedrock occur. Note that because topographic steady-state occurs when rock uplift rate is equal to the long-term incision rate E_{lt}, the absolute values of rock uplift rate and

steady-state instantaneous erosion rate differ by a factor of F_t. As before, to help ground the analysis in the range of physically reasonable values, we hold all other variables constant at South Fork Eel River reference site conditions (Table 1). Note also that we consider 11 of the 12 incision models discussed in the previous section; for clarity, we have omitted the version of the saltation–abrasion model that lacks the threshold of suspension term.

4.3.1. The influence rock uplift rate on steady-state channel slope

Fig. 6a shows the predicted steady-state channel slope as a function of rock uplift rate for the various incision models. As before, the reference site is indicated by an open circle. Over a range of rock uplift rate spanning more than four orders of magnitude, the slope predicted by the saltation–abrasion model varies by only slightly more than one order of magnitude. As rock uplift rate declines from the reference site value, the steady-state saltation–abrasion model slope declines slowly until reaching a nearly constant value, set by S_{D_s}, the threshold of motion slope. As rock uplift rate increases from the reference site value, the predicted slope increases rapidly, until reaching a maximum, denoted by an asterisk. The saltation–abrasion model predicts that steady-state cannot be achieved for rates of rock uplift any more rapid, given the reference site values of grain size, rock strength, and other variables held constant. This maximum possible incision rate occurs because of the tradeoff between the increase in particle impact energy with the decrease in impact frequency, with increasing transport stage. As described in detail in Sklar and Dietrich (2004), for sufficiently high shear stress, the derivative of the saltation–abrasion incision function with transport stage becomes negative. Thus, further increases in slope beyond the peak value cause incision rate to decline, rather than increase.

The relatively small change in steady-state channel slope predicted by the saltation–abrasion model over a very large range of rock uplift occurs in part because of the adjustment in the fraction of the bed exposed to erosive wear. This is shown in Fig. 6b, where the fraction of the bed covered, assumed to correspond to the relative sediment supply (Q_s/Q_c), is plotted against rock uplift rate. For low rock uplift rates, only small changes in bed cover are required to accommodate large changes in the steady-state incision rate. As rock uplift rate becomes relatively large, and begins to approach the maximum possible steady-state value, the extent of bedrock exposed on the channel bed increases more rapidly.

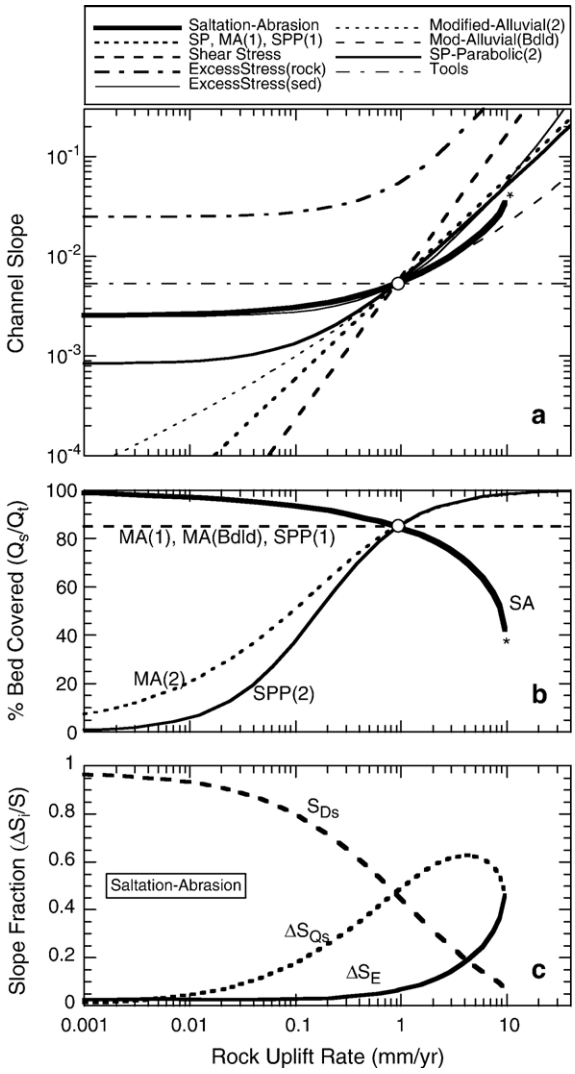

Fig. 6. Influence of variable rock uplift rate on: (a) steady-state channel slope for various models; (b) fraction of bed covered for models that account for cover effect; and (c) fraction of total slope due to the slope components responsible for grain motion (S_{D_s}), bedload sediment transport (ΔS_{Q_s}) and bedrock wear (ΔS_E) as predicted by the saltation–abrasion model. Reference site indicated by open circle. Maximum possible incision rate for saltation–abrasion model, for reference site conditions, indicated by asterisk.

The non-linear increase in steady-state channel slope with increasing rock uplift rate is best understood by considering the relative contributions of each of the slope components defined above to the total channel slope. Fig. 6c shows each of the slope components, normalized by the total channel slope, for the range of rock uplift rates. The threshold of motion component dominates the total slope for low values of rock uplift rate, but declines in importance as rock uplift becomes relatively rapid. Because increases in steady-state rock

uplift rate result in accelerated rates of erosion and sediment production in the upstream landscape, sediment supply increases linearly with rock uplift rate (for a constant bedload fraction of the total load F_b). This effect influences the increase in channel slope above S_{D_s} much more significantly than does the requirement that the channel incise at the rate of rock uplift. For relatively high rock uplift rates, ΔS_{Q_s} is the dominant control on channel slope. The slope increment responsible for bedrock incision ΔS_E grows rapidly as the peak erosion rate is approached, but is never the dominant slope component term. Overall, the saltation–abrasion model predicts that the effects of grain size and sediment supply primarily control steady-state channel slope, over the full range of rock uplift rates for which steady-state can be achieved by bedload abrasion.

The behavior of the saltation–abrasion model is fundamentally different from the stream power and shear stress models, as well as the linear forms ($n=1$) of the modified-alluvial and parabolic stream power incision models. Each of these models predicts a rapid and continuous decline in slope with reduced uplift rate, without any limit to how low the slope can become (Fig. 6a). Orders of magnitude variation in uplift rate are accommodated by orders of magnitude change in channel slope, and thus predicted topographic relief. This power law behavior is expected from the stream power and shear stress models. In contrast, the modified alluvial and parabolic stream power models explicitly include the cover effect and thus might be expected to predict changes in the extent of bed cover with changing erosion rate and sediment supply. However, as shown in Fig. 6b, the linear form of these models predicts a constant extent of bed cover because the reduction in sediment supply with reduced rock uplift rate is exactly matched by a reduction in sediment transport capacity. The bedload version of the modified alluvial model also predicts constant bed exposure despite large changes in rock uplift rate and sediment supply (Fig. 6a), however, this model closely follows the slope variation predicted by the saltation–abrasion model (Fig. 6a) because, as defined above, they share the same form of sediment transport relation (Eq. (4)).

The non-linear ($n=2$) forms of the modified-alluvial and parabolic stream power models do predict changes in bed cover with changing uplift rate, however the effect is opposite to that predicted by the saltation–abrasion model. As shown in Fig. 6b, these models predict that the fraction of the bed covered becomes increasingly small as uplift rate is reduced, approaching bare bedrock as erosion rate becomes negligibly small. This occurs in the case of the non-linear modified alluvial model because steady-state slope depends on erosion rate to a power less than unity in Eq. (41) (note that Q_s^2 appears in the denominator of the last term), so transport capacity declines more slowly than sediment supply as uplift rate is reduced. In the case of the non-linear parabolic stream power model, as uplift rate is reduced the predicted steady-state slope declines to a constant value, much like the saltation–abrasion model. However, unlike the threshold of motion slope, this constant slope value has no physical meaning, but is merely a mathematical artifact. At steady-state, erosion and sediment supply cancel in the first term within the parentheses of Eq. (45), and the resulting constant term is independent of grain size, sediment supply rate and rock uplift rate. Because slope remains large, sediment transport capacity remains high as uplift rate and sediment supply decline, and the fraction of the bed covered goes to zero.

The two versions of the excess shear stress model, with the critical shear stress term set alternatively by a rock detachment threshold or the threshold of sediment motion, both predict a non-linear variation in channel slope similar to the saltation–abrasion model. The sediment mobilization version closely tracks the saltation–abrasion model for low rock uplift rates where grain size is the dominant control on channel slope, but predicts a more rapid increase in slope for relatively high uplift rates as it approaches the power law behavior of the simple shear stress model. The rock detachment version of the excess shear stress model is exactly parallel, only shifted up by a factor set by the difference in the threshold value. Finally, the tools model predicts no dependence of steady-state channel slope on rock uplift rate. This surprising result occurs because the increase in the incision rate required to maintain steady state with increasing rock uplift rate is exactly balanced by the increase in tools provided by the increased sediment supply.

4.3.2. The influence of rock strength on steady-state channel slope

Fig. 7a shows the variation in predicted steady-state channel slope as a function of rock tensile strength for the various incision models. In this calculation, rock strength varies by a factor of 20, which corresponds to a 400-fold difference in rock resistance to abrasive wear (Sklar and Dietrich, 2001). For this range of rock resistance, which covers most competent lithologies encountered in tectonically active landscapes, the saltation–abrasion model predicts only subtle changes in steady-state channel slope. Unlike rock uplift rate, variations in rock strength do not change the steady-

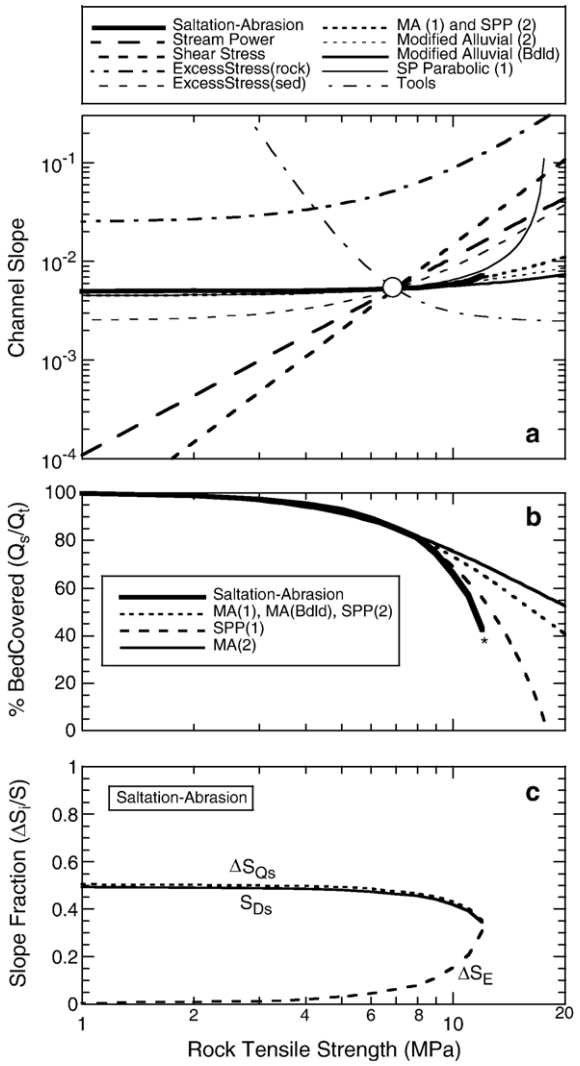

Fig. 7. Influence of variable rock tensile strength on: (a) steady-state channel slope for various models; (b) fraction of bed covered for models that account for cover effect; and (c) fraction of total slope due to the slope components responsible for grain motion (S_{D_s}), bedload sediment transport (ΔS_{Q_s}) and bedrock wear (ΔS_E) as predicted by the saltation–abrasion model. Reference site indicated by open circle. Maximum possible incision rate for saltation–abrasion model, for reference site conditions, indicated by asterisk.

state sediment supply rate, and thus only affect slope by requiring changes in the efficiency of the incision process. As shown in Fig. 7b, the efficiency of the bedload abrasion mechanism is increased in response to more resistant rock by increases in the extent of bedrock exposed in the channel bed. Because sediment supply and grain size are constant, only small increments in slope are required to reduce bed cover substantially. For the reference site values of grain size and sediment supply, the slope components due to these variables are coincidentally equal (Fig. 7c), and dominate the total slope except for the highly resistant rocks. Thus, for weak and moderate strength rocks, the channel slope is essentially independent of rock strength and is controlled by the requirement to mobilize and transport the supplied coarse sediment load. However, at the high end of the range of rock tensile strengths, the saltation–abrasion model predicts that bedload abrasion cannot erode efficiently enough to match the rate of rock uplift (for reference site conditions). Increases in channel slope above the peak value denoted by the asterisk in Fig. 7a would increase the extent of bedrock exposure, but not enough to compensate for the accompanying reduction in the frequency of particle impacts.

In contrast, models that do not include sediment effects, such as the stream power and shear stress models predict a simple power law dependence of steady-state channel slope on rock tensile strength (Fig. 7a). Models that include the cover effect, such as the linear and non-linear versions of the modified alluvial and parabolic stream power models, predict a narrow range of slopes over a wide range of rock strengths, because the constant sediment supply rate imposes a minimum slope which must be exceeded for incision to occur. As with the saltation–abrasion model, the reduced erosional efficiency as rock strength increases is offset by a corresponding increase in the fraction of the bed exposed (Fig. 7b), which is accomplished with small changes in channel slope. Counter-intuitively, the tools model predicts a decrease in slope with increasing rock strength. This occurs because for this model erosional efficiency is increased by increasing the frequency of particle impacts, which in the absence of a change in sediment supply rate, can only be accomplished by a reduction in shear stress, which reduces the saltation hop length.

4.3.3. The influence of the magnitude–frequency trade-off on steady-state channel slopes

In this calculation we vary the magnitude–frequency parameter F_t to evaluate how the steady-state channel slopes predicted by the various models vary with storminess. As described in detail in Section 2.2, above, when $F_t = 1.0$, discharge and coarse sediment occur continuously at the mean annual rates of water and sediment delivery from the upstream watershed. As F_t decreases, the magnitudes of both the high flow discharge and coarse sediment supply increase, while the duration decreases. Because in this approach discharge is partitioned into high and low flow components, but all coarse sediment is assumed to be transport only during the high flows, sediment

supply grows more rapidly than discharge as high-flow events become increasingly infrequent ($F_t \ll 1.0$). As before, all variables not affected by changes in F_t are held constant at South Fork Eel River reference site values.

Fig. 8a shows the variation in channel slope as a function of the high flow time fraction F_t for the various incision models. The slope predicted by the saltation–abrasion model is highest at the two extremes of the range of F_t, and reaches a minimum at the reference site value of F_t. The range of predicted slopes varies by about a factor of two. The slope is steepest for $F_t = 1.0$ because high flow discharge, and thus flow depth, are lowest, and a high slope value is needed to exceed the threshold of motion. As shown in Fig. 8b and c, at $F_t = 1.0$ the bed is nearly completely covered, and the total slope is dominated by the threshold of motion component S_{D_s}. Because the instantaneous erosion rate $E_i = E_{lt}/F_t$ ($= U_r/F_t$ for steady-state), E_i is minimized at $F_t = 1.0$ and the slope increment due to incision ΔS_E is also minimized.

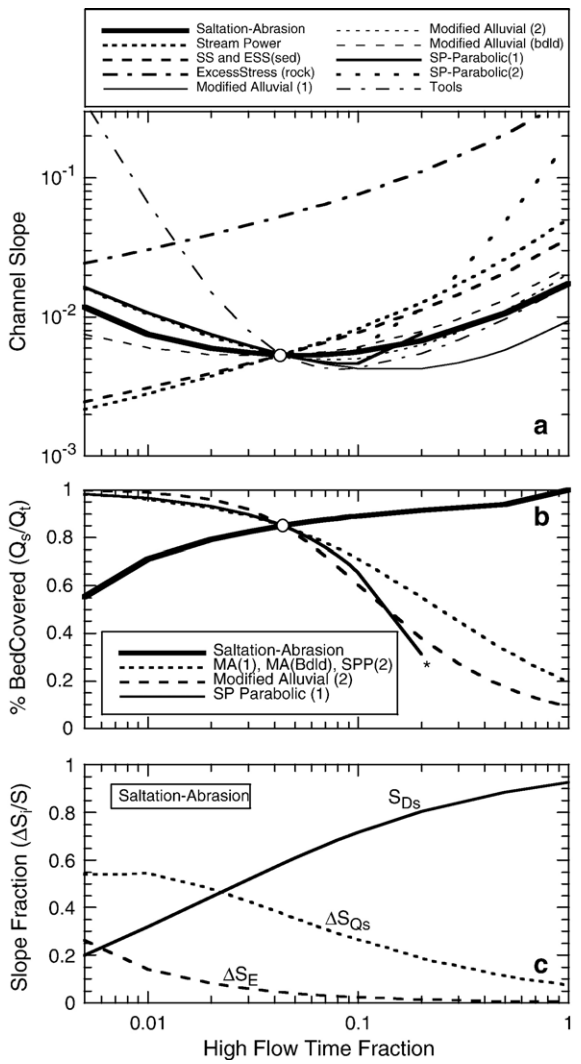

Fig. 8. Influence of variable high flow time fraction parameter on: (a) steady-state channel slope for various models; (b) fraction of bed covered for models that account for cover effect; and (c) fraction of total slope due to the slope components responsible for grain motion (S_{D_s}), bedload sediment transport (ΔS_{Q_s}) and bedrock wear (ΔS_E) as predicted by the saltation–abrasion model. Reference site indicated by open circle. Maximum possible incision rate for linear parabolic stream power model, for reference site conditions, indicated by asterisk.

The saltation–abrasion slope is also relatively steep for $F_t \ll 1.0$. For this highly 'stormy' representation of the distribution of discharges, the low frequency of high flow events results in very high coarse sediment supply and a high instantaneous incision rate. In order to transport this high load, the slope must be considerably steeper than the threshold of motion slope, and to incise at this rapid rate, exposed bedrock must occupy a large fraction of the channel bed (Fig. 8b). For these reasons, the total slope is dominated by ΔS_{Q_s} and ΔS_E (Fig. 8c). The predicted slope reaches a minimum at the reference site value of $F_t = 0.0437$ for the same reason that this value was selected in Section 2.2, because the product of discharge magnitude and duration is maximum at this value, resulting in the maximum net annual sediment transport capacity for a given slope. (Note that in the previous calculation slope was held constant, here slope is allowed to vary while long-term incision rate is held constant.)

Because the stream power and shear stress models do not account for the effects of sediment, those models predict a simple continuous increase in steady-state channel slope with increasing high flow time fraction (F_t). This results from a tradeoff between slope and discharge; as high flow discharge declines with increasing F_t, slope increases to compensate. The rate of slope increase is tempered by the accompanying decline in instantaneous incision rate with increasing F_t. The excess shear stress models follow the same pattern as the shear stress model, with the rock detachment version offset again by the assumed difference in threshold value. Most of the models that account for one or more of the effects of sediment on bedrock incision generally follow the pattern of slope variation predicted by the saltation–abrasion model, with slope maxima at either end of the range of F_t with a minimum at a moderate value of F_t. However, as with the previous calculation of steady-state slope as a function of rock uplift rate, the pattern of bed coverage predicted by the various versions of the modified

alluvial and parabolic stream power models is opposite that predicted by the saltation–abrasion model. As shown in Fig. 8b, those models predict large extents of bedrock cover during high magnitude, low frequency events ($F_t \ll 1$), and little alluvial cover for low magnitude, high frequency events ($F_t \sim 1$). The linear parabolic stream power model cannot maintain steady state for low bed coverage; the maximum possible steady-state value of F_t is indicated with an asterisk. This occurs due to a reversal in the sign of the derivative of the incision function with respect to flow intensity, as the incision function moves down into the tools-deprived region of the parabolic sediment supply effect (Fig. 3). Finally, the tools-based model shows an exaggerated version of the slope variation pattern of most of the other sediment-influenced models, but for the opposite reason. The slope predicted by the tools model is very high for $F_t \ll 1$ in order to offset the large increase in the frequency of bedload impacts, and consequent increase in incisional efficiency, caused by the high sediment supply rate.

4.3.4. Non-dimensional representation of saltation–abrasion model slope variation

An additional way of understanding the pattern of variation in steady-state channel slope predicted by the saltation–abrasion model in the three preceding calculations, is by plotting the associated path across the non-dimensional representation of the incision function surface. This is shown in Fig. 9, where, unlike the contour plots of Fig. 4, we plot contours of incision rate non-dimensionalized by grain diameter and rock tensile strength

$$E^* = \frac{E\sigma_T^2}{\rho_s Y (gD_s)^{3/2}} \tag{46}$$

as derived in Sklar and Dietrich (2004). The South Fork Eel River reference site is again indicated with an open circle. With this concise representation of the saltation–abrasion incision function, the calculated variation in slope with rock uplift rate and with the magnitude–frequency parameter F_t traverse the identical path. For slow rock uplift rates (U_r), or large high flow time fractions (F_t), the steady-state channel reach is just above the threshold of motion ($S \sim S_D$; Figs. 6c and 8c), with nearly complete bed coverage ($Q_s/Q_c \sim 1$; Figs. 6b and 8b), and relatively low instantaneous incision rate $\Delta S_E \ll S$ (Figs. 6c and 8c). As U_r increases, or F_t decreases, the channel plotting position in Fig. 9 climbs toward the peak of the functional surface, reflecting the increase in the instantaneous incision rate (E_i). At the maximum possible incision rate (asterisks), it is evident that extending the curve further by increasing transport stage would cause the plotting position to descend down the flank of the functional surface, and result in a reduced incision rate and a failure to maintain steady-state.

For the calculation of slope as a function of rock strength, the plotting position in Fig. 9 for weak rocks is $Q_s/Q_c \sim 1$ (Fig. 7b), but in this case $\tau^*/\tau_c^* > 1$ because sediment supply is constant, and $S_{D_s} \sim \Delta S_{Q_s}$ (Fig. 7c). As rock strength increases, the plotting position climbs to higher values of E^*, following a path of more subdued change in τ^*/τ_c^* that reflects the small change in predicted steady-state slope (Fig. 7a). Fig. 9 shows again that the peak possible steady-state slope occurs as the plotting position path is about to begin descending down the low relative supply flank of the functional surface. The difference in the plotting position paths, between the $S=f(U_r)$ or $S=f(F_t)$ cases and the $S=f(\sigma_T)$ case, is due to the fact that sediment supply varies with U_r and F_t but not with σ_T. The increase in sediment supply pushes the path for the U_r and F_t cases to a much higher transport stage to achieve the approximately same extent of bed exposure at the peak slope, than is required in the σ_T case where sediment supply is constant.

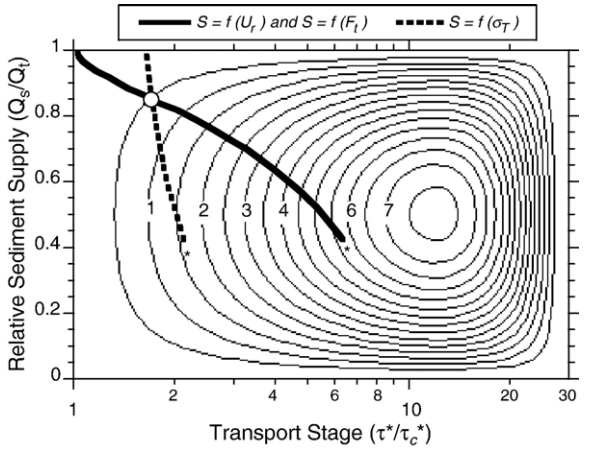

Fig. 9. Non-dimensional bedrock erosion rate ($E^* = E_i\sigma_T^2/\rho_s Y(gD_s)^{3/2} \times 10^{-15}$; contours, axis out of the page) as a function of transport stage and relative sediment supply, showing plotting position path for the calculation of steady-state channel slope predicted by the saltation–abrasion model shown in Figs. 6–8.

5. Discussion

The preceding analysis suggests that there is a hierarchy of factors controlling channel slope in

tectonically active landscapes that are in approximately topographic steady-state. The grain size of the coarse fraction of the total load is the dominant factor over a wide range of conditions, including weak to moderate strength rocks, low to moderate rock uplift rates, and relatively uniform to moderately 'stormy' discharge distributions. The supply rate of coarse sediments is the second most important factor in setting steady-state slopes, while bedrock wear itself is only a significant control for very resistant rocks and extremely rapid rates of rock uplift.

Given the importance of grain size in setting channel slopes, an obvious weakness of the saltation–abrasion model, as applied here, is the use of a single grain diameter to represent the effect of the wide range of grain sizes that may move as bedload through a reach of an actively incising channel. Explicitly accounting for grain size distributions would require use of bedload sediment transport relations that predict sediment flux for each grain size class (e.g. Parker, 1990). Also needed are new observations and insights into the role of mixed grain sizes in controlling the thresholds of alluviation and the relationship between sediment supply, transport capacity, and the partial coverage of bedrock. Preliminary wear rate measurements (*unpublished*) using mixed grain sizes in a bedrock abrasion mill suggest, however, that for relatively low sediment supply rates, the presence of a grain mixture has little effect. Total wear rates are similar to what would be obtained by a mass-weighted sum using data from uniform grain size runs.

Assessment of the morphologic implications of the saltation–abrasion model is limited by our lack of understanding of the controls on the grain size distribution of sediment supplied to the channel network by hillslopes. Here we have treated grain size as independent of all other variables, however, it is likely that grain size will covary with rock uplift rate, rock strength, and other variables such as discharge. Steady-state landscapes underlain by more resistant rocks, eroding more rapidly, or in more arid climates, are likely to produce and deliver to channels relatively coarser grain size distributions. Not only will grain size be affected, but the fraction of total load in the bedload size class F_b should be larger as well.

Further research is also needed to improve our understanding of the effects of episodic sediment supply on the extent of partial alluviation in bedrock channels. Although we have assumed here that stochastic variations in sediment supply can be effectively averaged over time, the bed condition of actively eroding rivers such as the South Fork Eel may be highly variable over an annual to decadal time scale (Howard, 1998). The sensitivity of the extent of alluviation to episodic sediment supply may be enhanced by non-linear effects in the relationship between relative sediment supply and the percentage of bed cover. As discussed in more detail in the development of the saltation–abrasion model (Sklar and Dietrich, 2004), there may be a threshold sediment supply required before any transient deposits of alluvium can form, and a threshold extent of bed cover above which a run away alluviation occurs, due to changes in bed roughness and bedload sediment transport efficiency.

The hierarchy of slope controlling factors identified by the saltation–abrasion model provides a useful framework for evaluating the utility of the other incision models discussed above. The most important sediment effect is the threshold of motion, which surprisingly is not explicitly included in any other published models, although versions of the excess shear stress model have been used without specifically linking the value of τ_c to sediment grain size (Tucker and Slingerland, 1997; Tucker and Bras, 1998). Treating τ_c as a rock strength dependent parameter potentially has the same effect in setting a minimum slope (Fig. 6a), however we know of no direct evidence for the existence of a general detachment threshold. As we noted previously (Sklar and Dietrich, 2004), bedrock abrasion mill experiments failed to detect a detachment threshold for the erosional mechanism of abrasion by sediment impacts.

The influence of sediment supply on the extent of bedrock exposure in the channel bed is the second-most important effect that consideration of sediment introduces to the bedrock incision problem. As we have argued previously (Sklar and Dietrich, 2001), partial bed coverage introduces an important degree of freedom for channel adjustment. As illustrated above (Figs. 6b, 7b and 8b), small changes in channel slope can result in large changes in the efficiency of bedrock incision, due to shifts in the percentage of bed alluviation. Interestingly, models that are intended to represent the cover effect, such as the modified alluvial and parabolic stream power models, can predict no adjustment in partial bed coverage with variable rock uplift rate, and can even predict patterns of bed cover adjustment opposite to those predicted by saltation–abrasion model (Fig. 6b).

The case of the non-linear parabolic stream power model illustrates a potential pitfall in developing geomorphic process models without a strong mechanistic basis. That model predicts an apparent threshold slope for low uplift rates, which, as described above, has no physical meaning. The non-linear version ($n=2$) was proposed to eliminate the computationally troublesome

upper limit to the range of possible erosion rates predicted by the linear version ($n=1$) of the parabolic stream power model (Fig. 8b). Unfortunately, choosing parameter values on the basis of mathematical convenience can lead to profoundly counter-intuitive model behavior as well as reasonable yet wholly artifactual results.

The tools effect is third in order of importance among sediment effects on bedrock incision rates. For example, the tools-based model, which includes the tools effect as well as the threshold of motion, predicts strongly counter-intuitive and highly divergent dependencies of slope on rock strength and uplift rate. On the other hand, the bedload version of the modified alluvial model, which includes the threshold of motion and cover effects but not the tools effect, is arguably the most likely among the other models discussed above to produce the results similar to those predicted by saltation–abrasion model. And only minor differences exist between the predictions of the published versions of the modified alluvial and parabolic stream power models, both of which include the cover effect while only the latter accounts for the tools effect.

Finally, the suspension effect is the least important of the four sediment effects in influencing predicted steady-state channel slopes. Although the version of the saltation–abrasion model lacking the suspension–extrapolation term was not tested here, the fact that the maximum possible bedload abrasion rate was encountered at low values of transport stage relative to the threshold of suspension (Fig. 9) indicates that the suspension effect is not responsible for the existence of that instability. As discussed in detail by Sklar and Dietrich (2004), the decline in incision rate with increasing shear stress is fundamentally due to the elongation of saltation trajectories, even without any shift in transport mode. Rather than being a computation annoyance, this result may be evidence of a real effect in river profile evolution. Over-steepening of tributary channels upstream of junctions could lead to hanging valleys, or formation of migrating knickpoints. These hypotheses illustrate the benefits of developing geomorphic process models beginning with the detailed mechanics, and remaining faithful to the original assumptions through the subsequent steps of scaling up and exploring morphologic implications.

6. Conclusion

We have demonstrated how the saltation–abrasion model, which was derived at the spatial and temporal scale of individual bedload sediment saltation impacts, can be scaled up for application at the scale of longitudinal profile evolution. Because the core model has no freely adjustable parameters, the additional parameters introduced in scaling up have explicit physical significance. As a result, the sensitivity of specific morphologic implications, such as predicted steady-state channel slope, to those parameter values can be meaningfully evaluated. Two important ideas are introduced in our treatment of the problem of balancing the tradeoffs between the magnitude and frequency of high flow events that transport bedload sediment and incise bedrock. First is the use of a real discharge record, and estimates of long-term mean denudation rates, from a reference field site, to make sure that the method respects the constraints that the total average annual runoff and sediment yield must be conveyed through a given reach of river. Second, because we recognize the contribution of low flow discharges to the annual water budget, we can rationally select the representative high flow magnitude and duration that most closely approximates the net effect of the full distribution of discharges in transporting bedload. We find that moderate magnitude discharges best represent the full distribution because low magnitude discharges fall below the threshold of motion, and high magnitude discharges occur so infrequently that the associated bedload sediment supply is too great to allow bedrock exposure in the channel bed.

Comparison of the behavior of the saltation–abrasion model with a range of other bedrock incision models, each of which fails to capture at least one of the four effects of sediment, reveals important differences with significant morphologic implications. Models that lack the threshold of motion over-predict incision rate for low shear stresses and under-predict the steady-state channel slope for low to moderate rock uplift rates and rock strengths. Models that lack the cover effect over-predict incision rate for high sediment supply rates, and fail to represent the degree of freedom in channel adjustment provided by partial bed coverage. Models that lack the tools effect over-predict incision rate for low sediment supply rates, and do not allow for the possibility that incision rate can decline for increases in shear stress above a peak value.

Two conceptual tools help clarify the controls on steady-state channel slope predicted by the saltation–abrasion model. The first is the idea that total slope can be considered a sum of components, each responsible for one of three tasks of a river channel at steady state, listed here in order of descending importance overall: mobilization of bed sediments, transport of supplied coarse sediment load, and incision into bedrock at the

rate of rock uplift. The second is the non-dimensional representation of the incision model as a function of transport stage and relative sediment supply. Using these tools we have shown that the influence of rock uplift rate, rock strength and the 'storminess' of the discharge distribution on steady-state slope are expressed primarily through their effect on relative sediment supply, which controls the extent of bed exposure in the channel bed.

Notation

A	upstream drainage area (km^2)
A_o	drainage area at channel head (km^2)
b	coefficient for change in Q_w with A ($m^3\ s^{-1}\ km^{-2p}$)
c	coefficient for change in W with Q_w (m^{1-3f}/s^f)
d	coefficient for change in A with x (km^{2-h})
D_o	grain diameter at channel head (m)
D_s	grain diameter (m)
E_i	instantaneous bedrock erosion rate (m/s)
E_{lt}	long-term bedrock erosion rate (mm/year)
E^*	non-dimensional erosion rate per unit rock resistance
f	exponent for change in W with Q_w
F_b	fraction of total load in coarse bedload size class
F_t	fraction of total time when high flow occurs
F_w	fraction of total runoff carried by high flows
g	gravitational acceleration (m/s^2)
h	exponent for change in A with x
K_f	tools (Foley, 1980) model efficiency ($m\ s^2/kg$)
K_h	tools (Howard et al., 1994) model efficiency ($m^{0.9}\ s^{1.5}\ kg^{-1}$)
K_{ma}	modified alluvial model efficiency (m/kg)
$K_{ma\text{-}b}$	bedload modified alluvial model efficiency (m/kg)
K_n	stream power modified alluvial model efficiency ($m^{2n+1}\ s^{-1}\ W^{-n}$)
K_p	parabolic stream power model efficiency ($m^{2n-1}\ W^{1-n}\ kg^{-1}$)
K_{qa}	stream power sediment transport coefficient ($kg\ m^2\ s^{-1}\ W^{-1}$)
k_v	saltation–abrasion rock resistance coefficient
K_γ	placeholder erosional efficiency coefficient
K_Ω	stream power model efficiency ($m^{1+n}\ s^{-1}\ W^{-n}$)
K_ω	unit stream power model efficiency ($m^{2n+1}\ s^{-1}\ W^{-n}$)
K_τ	shear stress model efficiency ($m\ s^{-1}\ Pa^{-1}$)
$K_{\tau\text{-cr}}$	excess shear stress (rock) model efficiency ($m\ s^{-1}\ Pa^{-1}$)
$K_{\tau\text{-cs}}$	excess shear stress (sediment) model efficiency ($m\ s^{-1}\ Pa^{-1}$)
I_r	impact rate per unit area per unit time ($1/m^2\ s$)
L_r	representative reach length (m)
N	number of discharges in flow record
m	rank of individual discharge
n	exponent in stream power and shear stress models
n_m	mannings channel roughness coefficient ($s/m^{1/3}$)
p	exponent for change in Q_w with A
P_{ne}	probability of non-exceedance
Q_s	sediment supply (kg/s)
Q_{sM}	mean annual sediment supply (kg/s)
Q_c	sediment transport capacity (kg/s)
Q_{cT}	total-runoff method sediment transport capacity (kg/s)
Q_{cH}	high-flow sediment transport capacity (kg/s)
Q_w	discharge (m^3/s)
Q_{wT}	representative discharge, total-runoff method (m^3/s)
Q_{wH}	representative discharge, high flow method (m^3/s)
Q_{wL}	residual low flow discharge, high flow method (m^3/s)
R_b	non-dimensional bouyant density
R_{ep}	particle Reynolds number
R_h	hydraulic radius (m)
S	channel slope
S_D	slope component for threshold of sediment motion
ΔS_{Q_s}	slope increment for transport of supplied sediment
ΔS_E	slope increment for erosion of bedrock
U_r	rock uplift rate (mm/year)
u^*	flow shear velocity (m/s)
W	channel width (m)
w_f	particle fall velocity (m/s)
x	distance downstream of channel head (km)
x_o	unchanneled distance (km)
Y	rock modulus of elasticity (MPa)
α	downstream fining exponent
$\sum Q_{cA}$	annual transport capacity summed over flow record (kg/year)
$\sum Q_{cH}$	annual transport capacity of representative high flow (kg/year)
γ	placehold flow intensity variable
λ	sediment porosity
ω	unit stream power (W/m^2)
Ω	stream power (W/m)
μ	viscosity of water ($kg\ m^{-1}\ s^{-1}$)
ρ_s	sediment density (kg/m^3)
ρ_w	water density (kg/m^3)
σ_T	rock tensile strength (MPa)
τ_b	mean boundary shear stress (Pa)

$\tau_{c\text{-}rock}$ rock strength-determined critical shear stress (Pa)
$\tau_{c\text{-}sed}$ sediment grain size-determined critical shear stress (Pa)
τ^* non-dimensional shear stress
τ_c^* non-dimensional critical shear stress
τ^*/τ_c^* transport stage

Acknowledgements

We thank G. Hauer, J. Kirchner, A. Luers, J. Roering, M. Stacey, J. Stock, and K. Whipple for stimulating and insightful discussions. Thoughtful comments by two anonymous reviewers helped to improve the manuscript. This work was supported by the National Center for Earth-Surface Dynamics, by NSF grant EAR 970608, and by a Switzer Environmental Fellowship to L.S.S.

References

Bathurst, J.C., 1993. Flow resistance through the channel network. In: Beven, K., Kirkby, M.J. (Eds.), Channel Network Hydrology. John Wiley & Sons, Chichester.

Beaumont, C., Fullsack, P., Hamilton, J., 1992. Erosional control of active compressional orogens. In: McClay, K.R. (Ed.), Thrust Tectonics. Chapman and Hall, New York, pp. 1–18.

Bezinge, A., 1987. Glacial meltwater streams, hydrology and sediment transport: the case of the Grande Dixence Hydroelectricity Scheme. In: Gardiner, V. (Ed.), International Geomorphology 1986, Part I, pp. 473–498.

Bitter, J.G.A., 1963. A study of erosion phenomena, part I. Wear 6, 5–21.

Bogaart, P.W., Tucker, G.E., de Vries, J.J., 2003. Channel network morphology and sediment dynamics under alternating periglacial and temperate regimes: a numerical simulation study. Geomorphology 54, 257–277.

Bras, R.L., 1990. Hydrology: An Introduction to Hydrologic Science. Addison Wesley, Reading, MA.

Brierley, G.J., Hickin, E.J., 1985. The downstream gradation of particle sizes in the Squamish River, British Columbia. Earth Surface Processes and Landforms 10, 597–606.

Brush, L.M., 1961. Drainage basins, channels, and flow characteristics of selected streams in Central Pennsylvania. Professional Paper-Geological Survey (U.S.) 282-F.

Buffington, J.M., Montgomery, D.R., 1997. A systematic analysis of eight decades of incipient motion studies, with special reference to gravel-bedded rivers. Water Resources Research 33, 1993–2029.

Bull, W.B., 1979. Threshold of critical power in streams. Geological Society of America Bulletin 90, 453–464.

Dietrich, W.E., 1982. Settling velocity of natural particles. Water Resources Research 18, 1615–1626.

Dietrich, W.E., Montgomery, D.R., 1998. Hillslopes, channels, and landscape scale. In: Sposito, G. (Ed.), Scale Dependence and Scale Invariance in Hydrology. Cambridge University Press, Cambridge, pp. 30–60.

Fernandez-Luque, R., van Beek, R., 1976. Erosion and transport of bed-load sediment. Journal of Hydraulic Research 14, 127–144.

Foley, M.G., 1980. Bedrock incision by streams. Geological Society of America Bulletin Part II, 91, 2189–2213.

Hack, J.T., 1960. Interpretation of erosional topography in humid temperate regions. American Journal of Science 258A, 80–97.

Head, W.J., Harr, M.E., 1970. The development of a model to predict the erosion of materials by natural contaminants. Wear 15, 1–46.

Howard, A.D., 1980. Thresholds in river regime. In: Coates, D.R., Vitek, J.D. (Eds.), The Concept of Geomorphic Thresholds. Allen and Unwin, Boston, pp. 227–258.

Howard, A.D., 1994. A detachment-limited model of drainage basin evolution. Water Resources Research 30, 2261–2285.

Howard, A.D., 1998. Long profile development of bedrock channels: interaction of weathering, mass wasting, bed erosion, and sediment transport. In: Tinkler, K., Wohl, E.E (Eds.), Rivers Over Rock: Fluvial Processes in Bedrock Channels. Geophysical Monograph Series, vol. 107. American Geophysical Union, Washington, DC, pp. 237–260.

Howard, A.D., Kerby, G., 1983. Channel changes in badlands. Geological Society of America Bulletin 94, 739–752.

Howard, A.D., Dietrich, W.E., Seidl, M.A., 1994. Modeling fluvial erosion on regional to continental scales. Journal of Geophysical Research 99, 13971–13986.

Kooi, H., Beaumont, C., 1996. Large-scale geomorphology: classical concepts reconciled and integrated with contemporary ideas via a surface processes model. Journal of Geophysical Research 101, 3361–3386.

Lavé, J., Avouac, J.P., 2000. Active folding of fluvial terraces across the Siwaliks Hills, Himalayas of central Nepal. Journal of Geophysical Research 105 (B3), 5735–5770. doi:10.1029/1999JB900292.

Lave, J., Avouac, J.P., 2001. Fluvial incision and tectonic uplift across the Himalayas of central Nepal. Journal of Geophysical Research 106 (B11), 26561–26591.

Leopold, L.B., 1994. A View of the River. Harvard University Press, Cambridge. 298 pp.

Mackin, J.H., 1948. Concept of the graded river. Geological Society of America Bulletin 59, 463–512.

Merritts, D., Bull, W.B., 1989. Interpreting Quaternary uplift rates at the Mendocino triple junction, northern California, from uplifted marine terraces. Geology 17, 1020–1024.

Moglen, G.E., Bras, R.L., 1995. The effect of spatial heterogeneities on geomorphic expression in a model of basin evolution. Water Resources Research 31, 2613–2623.

Montgomery, D.R., Dietrich, W.E., 1988. Where do channels begin? Nature 336, 232–234.

Montgomery, D.R., Dietrich, W.E., 1992. Channel initiation and the problem of landscape scale. Science 255, 826–830.

Morris, P.H., Williams, D.J., 1999. A worldwide correlation for exponential bed particle size variation in subaerial aqueous flows. Earth Surface Processes and Landforms 24, 835–847.

Ohmori, H., 1991. Change in the mathematical function type describing the longitudinal profile of a river through an evolutionary process. Journal of Geology 99, 97–110.

Parker, G., 1990. Surface-based bedload transport relation for gravel rivers. Journal of Hydraulic Research 28 (4), 417–436.

Rouse, H., 1937. Modern conceptions of the mechanics of turbulence. Transactions of the ASCE 90, 463–543.

Schumm, S.A., 1973. Geomorphic thresholds and complex response of drainage systems. In: Morisawa, M. (Ed.), Fluvial Geomorphology. Publications in Geomorphology, Binghamton University (SUNY), pp. 299–310.

Seidl, M.A., Dietrich, W.E., 1992. The problem of channel erosion into bedrock. In: Schmidt, K.H., de Ploey, J. (Eds.), Functional Geomorphology. Catena Suppl., vol. 23, pp. 101–124.

Sklar, L.S., Dietrich, W.E., 1998. River longitudinal profiles and bedrock incision models: stream power and the influence of sediment supply. In: Tinkler, K., Wohl, E.E. (Eds.), Rivers Over Rock: Fluvial Processes in Bedrock Channels. Geophysical Monograph Series, vol. 107. American Geophysical Union, Washington, DC, pp. 237–260.

Sklar, L.S., Dietrich, W.E., 2001. Sediment and rock strength controls on river incision into bedrock. Geology 29, 1087–1090.

Sklar, L.S., Dietrich, W.E., 2004. A mechanistic model for river incision into bedrock by saltating bedload. Water Resources Research 40, W06301. doi:10.1029/2003WR002496.

Snow, R.S., Slingerland, R.L., 1987. Mathematical modeling of graded river profiles. Journal of Geology 95, 15–33.

Stock, J.D., Montgomery, D.R., Collins, B.D., Dietrich, W.E., Sklar, L. S., 2005. Field measurements of incision rates following bedrock exposure: implications for process controls on the long profiles of valleys cut by rivers and debris flows. Geological Society of America Bulletin 117, 174–194. doi:10.1130/B25560.1.

Tomkin, J.H., Brandon, M.T., Pazzaglia, F.J., Barbour, J., Willett, S.D., 2003. Quantitative testing of bedrock incision models, Clearwater River, WA. Journal of Geophysical Research 108 (B6), 2308. doi:10.1029/2001JB000862.

Tucker, G.E., Bras, R.L., 1998. Hillslope processes, drainage density, and landscape morphology. Water Resources Research 34, 2751–2764.

Tucker, G.E., Bras, R.L., 2000. A stochastic approach to modeling the role of rainfall variability in drainage basin evolution. Water Resources Research 36, 1953–1964.

Tucker, G., Slingerland, R., 1994. Erosional dynamics, flexural isostasy, and long-lived escarpments: a numerical modeling study. Journal of Geophysical Research 99, 12229–12243.

Tucker, G.E., Slingerland, R.L., 1996. Predicting sediment flux from fold and thrust belts. Basin Research 8, 329–349.

Tucker, G.E., Slingerland, R., 1997. Drainage basin responses to climate change. Water Resources Research 33 (8), 2031–2047.

Tucker, G.E., Whipple, K.X., 2002. Topographic outcomes predicted by stream erosion models: sensitivity analysis and intermodel comparison. Journal of Geophysical Research 107 (B9), 2179.

van der Beek, P., Bishop, P., 2003. Cenozoic river profile development in the Upper Lachlan catchment (SE Australia) as a test of quantitative fluvial incision models. Journal of Geophysical Research 108 (B6), 2309.

Whipple, K.X., Tucker, G.E., 1999. Dynamics of the stream-power river incision model: implications for height limits of mountain ranges, landscape response timescales, and research needs. Journal of Geophysical Research 104B, 17661–17674.

Whipple, K.X., Tucker, G.E., 2002. Implications of sediment-flux-dependent river incision models for landscape evolution. Journal of Geophysical Research, [Solid Earth] 107, 2039.

Whipple, K.X., Hancock, G.S., Anderson, R.S., 2000. River incision into bedrock: mechanics and relative efficacy of plucking, abrasion, and cavitation. Geological Society of America Bulletin 112, 490–503.

Wiberg, P.L., Smith, J.D., 1985. A theoretical model for saltating grains in water. Journal of Geophysical Research 90 (C4), 7341–7354.

Willett, S.D., 1999. Orogeny and orography: the effects of erosion on the structure of mountain belts. Journal of Geophysical Research 104, 28957–28981.

Willgoose, G., Bras, R.L., Rodriguez-Iturbe, I., 1991. A coupled channel network growth and hillslope evolution model 1. Theory. Water Resources Research 27, 1671–1684.